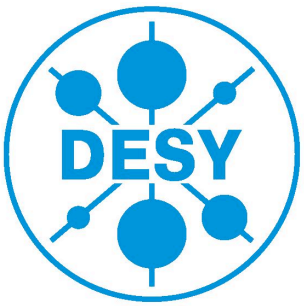

Estimation of charm and beauty quark-masses using data from HERA I + II

Philipp Henkenjohann, University of Bielefeld, Germany

September 11, 2014

Abstract

Jet, $b\bar{b}$ and $c\bar{c}$ cross sections measured at HERA are used for an estimation of α_s, m_c and m_b. The results are $\alpha_s = 0.118 \pm 0.001$, $m_c = 1.46 \pm 0.05$ (next to leading order), 1.43 ± 0.06 (next to next to leading order) and $m_b = 4.4 \pm 0.2$ GeV. These values are used for a determination of the experimental, parametrization and model uncertainty of the parton density functions which are fitted by using the mentioned data.

Contents

1 Introduction

Between 1992 and 2007 the experiments H1 and ZEUS gathered data from deep inelastic scattering (DIS) of electrons and positrons off protons at the HERA collider at DESY in Hamburg. Due to the large amount of collected data of about 1 fb^{-1} the H1 and ZEUS collaborations are still analyzing this data. From this data so called parton density functions (PDF's) can be determined along with several parameters related to QCD, such as the strong coupling constant α_s or the quark-masses. These PDF's can be used to analyze data from other experiments, for instance experiments at LHC. In this report estimations of the strong coupling constant α_s, the charm and beauty quark-masses using new combined data (unpublished) and data sensitive to $c\bar{c}$, $b\bar{b}$ and jet production are presented [1, 2, 5, 6, 7, 8, 9]. In addition PDF uncertainties determined by using the new data are shown in the end of the report.

2 Theory of deep inelastic scattering

In this section a rather brief and schematic introduction to the theoretical description of DIS is given. The emphasis is more on the physical ideas than on the actual calculations that have to be made in order to end up with a useful formula for the cross section of DIS processes. The following section is based on [3].

2.1 The quark-parton model

As we know today the proton is not an elementary particle but consists of two u-quarks and one d-quark. According to the theory of QCD these quarks are held together by the mediators of the strong force, the so-called gluons. Naively one would therefore guess that the quarks in the proton are not free. In fact we can describe the quarks in the proton as free particles in some special situations, though. This is due to a peculiarity of QCD: It is a non-Abelian gauge theory. As we know from QED the coupling constants of quantum field theories are actually not constant but have different values at different energies or corresponding length scales. The peculiarity of QCD then is the fact that the strong coupling constant decreases with increasing energy while the electromagnetic coupling constant does just the other way around. In this sense QCD is a completely different theory than QED which can be traced back to the properties of the underlying gauge group, as already mentioned. Having this in mind we can now argue that the quarks in the proton are approximately free particles since they are confined to a length scale of 1 fm. Of course this has to be established experimentally but in the end indeed this turns out to be the case.
Now we can go a step further and introduce the quark-parton model which was actually introduced by R. Feynman in 1969 even before QCD and all the knowledge mentioned so far were established. He invented this model in order to explain a behavior called Bjorken-scaling in DIS-experiments which will not be explained at this point. The quark-parton model describes the proton as made out of constituents called partons which can

be quarks but gluons as well. All these partons contribute to the properties of the proton for example the proton's charge or momentum. Since we assume the partons to be free within the proton we can describe the scattering of an electron off an proton by the scattering of an electron off an quark. In first order perturbation the electron does not interact with the gluons since the electron does not carry any color charge and the gluon does not carry any electric charge. Therefore electron-quark scattering suffices to describe the process at this level of accuracy. Let k and p be the 4-momenta of the incoming electron respectively the incoming quark. After the collision their 4-momenta are k' and p'. The electric charge of the electron is e and of the quark is e'. In first order perturbation theory this process is mediated by a virtual photon with 4-momentum-squared

$$q^2 = -Q^2 = (k - k')^2 . \tag{1}$$

The centre-of-mass energy squared is given by

$$s = (k + p)^2 \tag{2}$$

and one further kinematic variable is defined as

$$y = \frac{p \cdot q}{p \cdot k}. \tag{3}$$

The unpolarized differential cross-section for this process can be calculated to be

$$\frac{\mathrm{d}\sigma}{\mathrm{d}y} = \frac{e^2 e'^2}{8\pi Q^4} \left[1 + (1 - y)^2\right] s. \tag{4}$$

If we want to put this process in the context of DIS we have to take into account that the momentum of the quark is not experimentally accessible. We only know the quark must carry a fraction x of the four-momentum p of the proton which in contrast is measurable. Evaluating the above cross-section in terms of this new variable x we get

$$\frac{\mathrm{d}\sigma}{\mathrm{d}y} = \frac{2\pi\alpha^2}{Q^4} \left[1 + (1 - y)^2\right] x s e_\mathrm{i}^2 \tag{5}$$

where α is the fine structure constant and i denotes the quark type. A Feynman diagram of this process is shown in Fig. 1.

But we still have a problem: We do not know with which quark in the proton the electron will interact. To overcome this we introduce distribution functions $q_\mathrm{i}(x)$ which give the probability for the struck quark to be of type i and to carry the fraction x of the proton's momentum p. The momentum distribution is then $xq_\mathrm{i}(x)$ and will be referred to as PDF. Using the PDF's we end up with the following cross-section

$$\frac{\mathrm{d}^2\sigma}{\mathrm{d}x\mathrm{d}Q^2} = \frac{2\pi\alpha^2}{xQ^4} \left[1 + (1 - y)^2\right] \sum_\mathrm{i} e_\mathrm{i}^2 x q_\mathrm{i}(x) \tag{6}$$

Note that the probabilities for scattering with each of the quark types with a given momentum xp are summed incoherently, that is not the amplitudes are summed but

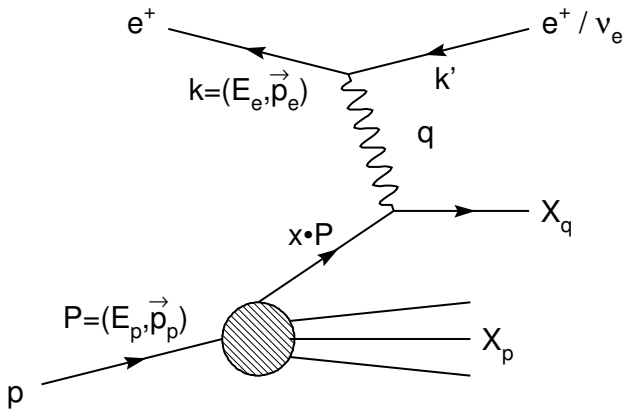

Figure 1: DIS is shown in terms of the quark-parton model. A parton carrying a fraction x of the proton's momentum interacts with the virtual photon emitted by the incoming positron. This Feynman diagram is leading order.

the probabilities themselves. This is justified by the assumption of free non-interacting quarks in the proton.
On the other hand one can deduce a general formula for the cross section of electron proton scattering without assuming the quark-parton model. Then the cross section takes on the form

$$\frac{\mathrm{d}^2\sigma}{\mathrm{d}x\mathrm{d}y} = \frac{4\pi\alpha^2 s}{Q^4}\left[xy^2 F_1(x,y) + (1-y)\,F_2(x,y)\right] \tag{7}$$

which can be rewritten by defining $F_\mathrm{L} = F_2 - 2xF_1$ and $Y_+ = 1 + (1-y)^2$ as

$$\frac{\mathrm{d}^2\sigma}{\mathrm{d}x\mathrm{d}Q^2} = \frac{2\pi\alpha^2}{xQ^4}\left[Y_+ F_2\left(x,Q^2\right) - y^2 F_\mathrm{L}\left(x,Q^2\right)\right]. \tag{8}$$

The functions F_1, F_2 and F_L are called structure functions. Comparing this with (5) we can immediately deduce

$$F_\mathrm{L}\left(x,Q^2\right) = 0 \tag{9}$$

and

$$F_2\left(x,Q^2\right) = \sum_\mathrm{i} e_\mathrm{i}^2 x q_\mathrm{i}(x)\,. \tag{10}$$

The fact that F_2 is independent of Q^2 is called Bjorken-scaling which is only valid for large Q^2. This is compatible with the quark-parton model which also is only valid for sufficiently large Q^2 in order to allow the assumption of free quarks in the proton.

2.2 Improved quark-parton model

So far we only considered the DIS to be mediated by a photon. At sufficiently high Q^2 we could also have a Z or $W^{\pm}$ boson acting as the mediator. Referring to the charge of the interchanged boson we can classify DIS processes as neutral current DIS (NC) or charged current DIS (CC). If we also consider the lepton type we end up with four different classes of DIS, namely $e^{\pm}$pNC/$e^{\pm}$pCC. The cross sections derived so far will be of course different for these different classes of processes but nevertheless the idea remains the same.
Experimentally we know that the final state of DIS consists not always again of lepton and proton. There are also a large number of events where the final state consists of hadronic jets. These final states cannot be explained by the quark-parton model introduced so far since there is no mechanism for hadron production yet. The solution to this problem is to apply QCD on DIS, in particular on the interaction between electron and quark. Doing this one has to take gluon radiation into account which finally leads to the production of quark-antiquark-pairs. Via this mechanism also other hadronic particles can be produced which all together constitute the observed jets. An example for such a process is shown in Fig. 2.

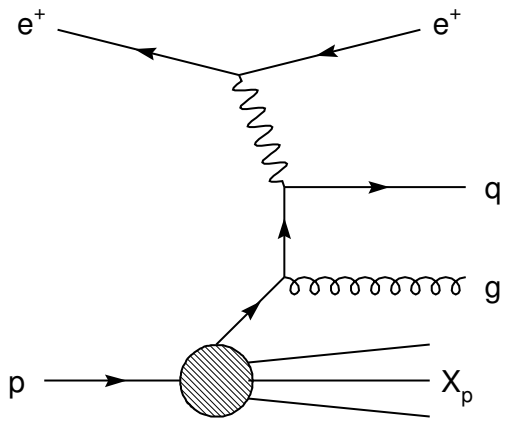

Figure 2: In this Feynman diagram a QCD process is included in DIS. The gluon can produce quark-antiquark-pairs which make up a jet. In higher order diagrams there can be several of these gluons.

By this approach it turned out experimentally that the two u-quarks and the d-quark are not sufficient to describe the proton properly. If one summed the momenta of the three quarks they did not add up to the momentum of the proton. In fact there was some amount of momentum missing. Therefore the notion of sea-quarks and sea-gluons was introduced in order to account for the missing momentum. Due to charge conservation the sea-quarks can only occur in quark-antiquark-pairs while there is no such restriction to the sea-gluons. To distinguish the "normal" quarks from the sea-quarks these are called valence-quarks. Now all these additional partons of the proton can also contribute

to DIS which results again in improved formulas for the cross sections. In general the cross section takes on the form

$$\sigma\left(x, Q^2\right) = \sum_{\mathrm{i}} \int_0^1 \mathrm{d}z \int_0^1 \mathrm{d}\xi f_{\mathrm{i}}\left(\xi\right) \delta\left(x - z\xi\right) \hat{\sigma}\left(z, Q^2\right), \tag{11}$$

where f_{i} are the distribution functions for the different partons labeled by i. The cross section $\hat{\sigma}$ describes the hard-scattering process that occurs between the incoming lepton and a parton.
Now the next step would be to extract the PDF's from the measured data. Since there is no a prori given analytic form for the PDF's one have to guess a reasonable form. There exist several ansatzes but there are some properties they all should share. For instance there are several sum rules which come from imposing that the parton's charge or momentum should sum up to the proton's charge or momentum and so on. Due to QCD the PDF's change with the energy scale Q^2. That means if we parametrize a PDF at a certain scale we have to evolve it to the scale of a certain event from the experiment in order to compare them. This is done by the DGLAP equations which were developed by Dokshitzer, Gribov, Lipatov, Altarelli and Parisi.

2.3 Heavy flavour schemes

There are various possibilities to treat the heavy flavour quarks, that is charm and beauty quark, in the theoretical calculations. In the following a brief description of three of them taken from [2] is given.

2.3.1 Zero mass variable flavor number scheme (ZM-VFNS)

In this scheme a threshold at $Q^2 \approx m^2_{\mathrm{c,\,b}}$ is introduced. Below this threshold the production cross section for this quark flavour is taken to be zero and the quark is excluded from the parton evolution. Above the threshold the quark mass is set to zero in all calculations and the corresponding PDF is determined. The LO process for the production in this scheme is the quark-parton-model like scattering.

2.3.2 Fixed flavour number scheme (FFNS)

In the FFNS the quark is treated as massive at all scales but not as a parton of the proton. Therefore the LO contribution for the production is gluon-gluon-fusion in hard scattering processes.

2.3.3 General mass variable flavour scheme (GM-VFNS)

This scheme is a combination of the previous two. In the low Q^2 region where masses have a large effect the FFNS is used. On the other hand at high Q^2 the ZM-VFNS is used. In the intermediate region of Q^2 an interpolation between these schemes is applied.

3 HERAFitter

HERAFitter is an open source platform [4] designed to extract the PDF's from various data sets using various theory models. For this purpose the whole theory outlined above is implemented in the code also using several external already available programmes such as MINUIT or QCDNUM. HERAFitter offers a whole variety of possible setups for the fit which mainly can be controlled via the steering file. First of all this is the file where the experimental input, given as specially formatted datafiles, is declared to the programme. Besides a lot of other settings such as the order of calculation, the Q^2-cut-off at which data is taken into account, the starting scale for the PDF's or the χ^2-definition can be controlled here. Besides these also the heavy flavor scheme can be changed in the steering file. One GM-FVNS was implemented by R.Thorne (RT OPT) which is used throughout this report. Another important file is the minuit file in which all the variables for the parametrization of the PDF's are defined and given starting values and step sizes used for the fit. One can also free the strong coupling constant α_s or the strange fraction f_s of the sea-quarks in the steering file. In the ewparam file electroweak constants are defined, for instance the mass of the quarks or the Weinberg angle. In addition to the actual fit of the PDF's HERAFitter is capable to produce plots of these. With some additional work it is also possible to make HERAFitter determine experimental, theoretical and model uncertainties of the fits and visualize in the plots.

4 Estimation of α_s

Before dealing with the quark-masses we can also have a look at the strong coupling constant α_s which can be determined by doing several fits with different values of α_s. The resulting χ^2-values can be plotted against the corresponding α_s. This procedure is also called a scan of α_s or in general of any variable that is input for the fit. For the optimal value of the variable we expect to observe a minimum of the χ^2. This minimum can be determined by fitting a quadratic polynomial to the points in the described plots. The 1σ-error is equal to the distance to the minimum which corresponds to a change of $\Delta\chi^2 = 1$. If the polynomial is parametrized by

$$f(x) = a_0 + a_1 x + a_2 x^2 \tag{12}$$

the result of the measurement is

$$x_0 = -\frac{a_1}{2a_2} \pm \frac{1}{\sqrt{a_2}}. \tag{13}$$

The α_s-scan is done with 14 free parameters for the parametrization of the PDF's, a minimum Q^2-cut at 3.5 GeV^2 and next to leading order (NLO) calculation. All in all two scans are done: One with inclusive NC + CC data (inclusive data) and one with inclusive data and data with jet cross section measurements (jet data) from [5, 6, 7, 8, 9]. In Fig. 3(a) and (b) the results are shown.

One can see very clearly that the jet data increases the sensitivity to α_s. Without jet data the sensitivity is too low to do a reasonable estimation of the optimal value. From the scan with jet data it follows $\alpha_s = 0.118 \pm 0.001$. This optimal value will be used in the following for the scans of the beauty and charm quark-mass.

5 Estimation of quark-masses

In this section the goal is to check the sensitivity of inclusive data to the masses of the charm and beauty quark. With charm and beauty data charm and beauty cross section measurements are meant. The procedure is the same for the charm and beauty quark-mass: Several scans are done by changing the mass in the ewparam file. This is done for a minimum Q^2 of 3.5 GeV^2 and 10.0 GeV^2, for NLO and next to next to leading order (NNLO) calculation and finally for 14 and 15 free parameters for the parametrization of the PDF's.

5.1 The beauty quark-mass

For the estimation of the beauty quark-mass we use, as already mentioned, the new inclusive data and the beauty cross section measurements [1]. First of all we can convince ourselves of the sensitivity of the data to the beauty mass by comparing scans using both data and using the inclusive data only. This is shown in Fig. 4. In the inclusive data only scan there is a straight line while the scan using both data has a clear minimum which shows the claimed sensitivity to m_b.
The next step is a determination of the mass from the scan. This mass will be used in PDF fits as an optimal mass in RT OPT heavy mass scheme. For this purpose several scans according to the setups mentioned above were performed. The results are shown in Fig. 5 and 6.
The first thing worth mentioning is the fact that the points of all six scans behave very much like a quadratic polynomial. Note that the NNLO fits with $Q^2 > 3.5$ GeV^2 were not performed because the beauty data begins only at values greater than 10.0 GeV^2. Therefore and due to the very low sensitivity of the inclusive data the missing scans should not differ much from the ones shown, which is shown for NLO in Fig. 5(a) and (b). Besides this behavior can be also seen from the plots at NLO. The values for m_b obtained here lie between 4.41 GeV and 4.46 GeV. The error is either 0.16 GeV or 0.17 GeV. The results are consistent. In particular the number of parameters seems not to have any influence on the scans. In fact the results of the NNLO scans are exactly the same. Hence a reasonable value for m_b is 4.4 GeV to be used in PDF fits with an error of roughly 0.2 GeV.

5.2 The charm quark-mass

For the scans of the charm-mass inclusive and charm data [2] are used. Besides the beauty quark-mass is set to 4.4 GeV which was estimated to be the optimal value in the

Variation	Standard Value	Lower Limit	Upper Limit
f_s	0.4	0.3	0.5
m_c(NLO) [GeV]	1.46	1.40	1.52
m_c (NNLO) [GeV]	1.43	1.37 ($Q_0^2 = 1.86$ GeV^2)	1.49
m_b [GeV]	4.4	4.15	4.65
Q^2_{min} [GeV^2]	10.0	7.5	12.5
Q^2_{min} [GeV^2]	3.5	2.5	5.0
Q_0^2 [GeV^2]	1.9	1.6	2.2 ($m_c = 1.49$ GeV)

Table 1: Standard values of input parameters and the variations considered.

RT OPT heavy flavor scheme in the previous section. The results are shown in Fig. 7 and 8.
With 14 parameters at NLO both scans with $Q^2 > 3.5$ GeV^2 and $Q^2 > 10.0$ GeV^2 give rise to a mass of about 1.46 GeV which is shown in Fig. 7(a) and (b). This picture changes if one consideres NNLO. Here the two Q^2-cuts lead to different mass estimations with a difference of 0.6 GeV. There is no detailed explanation for this behaviour yet but obviously the NNLO calculations are sensitive to the Q^2-cut.
With 15 parameters the situation does not change much. The estimation of the mass is slightly shifted to larger values at NNLO but the difference is negligible compared to the errors. At NNLO the optimal mass is then 1.43 ± 0.06 GeV using the 14 parameter scan with $Q^2 > 3.5$ GeV^2 shown in Fig. 7(c) while the NLO scans give rise to $m_c = 1.46 \pm 0.05$ GeV. Both values at NLO and NNLO are still compatible within the errors.

6 PDF uncertainties

In this section the uncertainties of the PDF's will be examined. There are three main sources of uncertainties: experimental, model and parametrization uncertainties. In the following model and parametrization uncertainties will be introduced in the context of PDF's.

6.1 Model and parametrization uncertainties

Model uncertainties and parametrization uncertainties of the central fit solution are evaluated by varying the input assumptions. The variation of numerical values chosen for the central fit is specified in Table 1.
The variation of f_s is chosen to span the ranges between a suppressed strange sea as determined in [10, 11] and an unsuppressed strange sea [12]. The variation of m_c is taken from [2]. This allows a considerably reduced uncertainty due to m_c variation as compared to the HERAPDF1.0 analysis. The variation of m_b is taken from reference [10].
The difference between the central fit and the fits corresponding to model variations of m_c, m_b, f_s, Q^2_{min} are added in quadrature, separately for positive and negative deviations, and represent the model uncertainty of the HERAPDF2.0 set.

The variation in Q_0^2 is regarded as a parametrization uncertainty, rather than a model uncertainty. Variation of the number of terms in the polynomial that describes the PDF's is also considered for each fitted parton distribution. In practice none of these have significantly different PDF shapes from the central fit.
The difference between the parametrization variations and the central fit is stored and an envelope representing the maximal deviation at each x value is constructed to represent the parametrization uncertainty. This parametrization uncertainty should be regarded as indicative rather than exhaustive. The total PDF uncertainty is obtained by adding in quadrature experimental, model and parametrization uncertainties.
In summary, the HERAPDF2.0 analysis uses a consistent data set with small correlated systematic uncertainties and applies the conventional χ^2 tolerance, $\Delta\chi^2 = 1$, when determining the experimental uncertainties on the PDFs. This data set includes four different processes, NC and CC, e^+p and e^-p scattering, such that there is sufficient information to extract $x\bar{U}, x\bar{D}, xd_v, xu_v$ PDFs and the gluon PDF from the scaling violations. The NC e^+p data includes data at different centre-of-mass energies such that different values of y are accessed at the same x, Q^2. This makes the data sensitive to F_L and thus gives further information on the low-x gluon distribution.

6.2 Results

The uncertainties have been determined for a variety of setups for the fits. For each setup the PDF's are evolved to six different Q^2-values and are plotted. First of all only inclusive data is taken into account for NLO as well as NNLO. For each of these the Q^2-cut is set equal to 10 GeV^2 and then equal to 3.5 GeV^2. The corresponding plots are shown in Fig. 9 to 12. The remaining plots are done by adding jet and charm data at NLO. Again the two Q^2-cuts at 10 GeV^2 and 3.5 GeV^2 are done with a free α_s and a fixed $\alpha_s = 0.118$. The results are shown in Fig. 13 to 16.

References

[1] H. Abramowicz *et al.* [ZEUS Collaboration], "Measurement of beauty and charm production in deep inelastic scattering at HERA and measurement of the beauty-quark mass," arXiv:1405.6915 [hep-ex].

[2] H. Abramowicz *et al.* [H1 and ZEUS Collaborations], "Combination and QCD Analysis of Charm Production Cross Section Measurements in Deep-Inelastic ep Scattering at HERA," Eur. Phys. J. C **73** (2013) 2311 [arXiv:1211.1182 [hep-ex]].

[3] A. Cooper-Sarkar, R. Devenish, "Deep Inelastic Scattering", Oxford University Press (2003).

[4] www.wiki-zeuthen.desy.de/HERAFitter

[5] V. Andreev *et al.* [H1 Collaboration], "Measurement of Multijet Production in ep Collisions at High Q^2 and Determination of the Strong Coupling α_s," arXiv:1406.4709 [hep-ex].

[6] H. Abramowicz *et al.* [ZEUS Collaboration], "Inclusive dijet cross sections in neutral current deep inelastic scattering at HERA," Eur. Phys. J. C **70** (2010) 965 [arXiv:1010.6167 [hep-ex]].

[7] S. Chekanov *et al.* [ZEUS Collaboration], "Inclusive jet cross-sections in the Breit frame in neutral current deep inelastic scattering at HERA and determination of α_s," Phys. Lett. B **547** (2002) 164 [hep-ex/0208037].

[8] T. Kluge [H1 Collaboration], "Inclusive Jet Production in DIS at High Q^2 and Extraction of the Strong Coupling," arXiv:0707.4057 [hep-ex].

[9] F. D. Aaron *et al.* [H1 Collaboration], "Jet Production in ep Collisions at Low Q^2 and Determination of α_s," Eur. Phys. J. C **67** (2010) 1 [arXiv:0911.5678 [hep-ex]].

[10] A. D. Martin, W. J. Stirling, R. S. Thorne and G. Watt (2009).

[11] P. M. Nadolsky, H. L. Lai, Q. H. Cao, J. Huston, J. Pumplin, D. Stump, W. K. Tung and C.-P. Yuan, "Implications of CTEQ global analysis for collider observables," Phys. Rev. D **78** (2008) 013004 [arXiv:0802.0007 [hep-ph]].

[12] G. Aad *et al.* [ATLAS Collaboration], "Determination of the strange quark density of the proton from ATLAS measurements of the $W \to \ell\nu$ and $Z \to \ell\ell$ cross sections," Phys. Rev. Lett. **109** (2012) 012001 [arXiv:1203.4051 [hep-ex]].

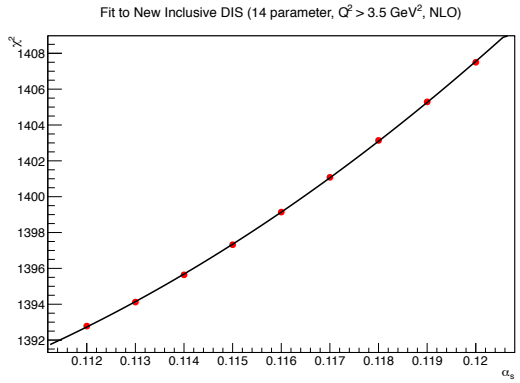

(a) α_s-scan using 14 parameter, $Q^2 > 3.5$ GeV^2 and NLO calculation. There is very low sensitivity to α_s.

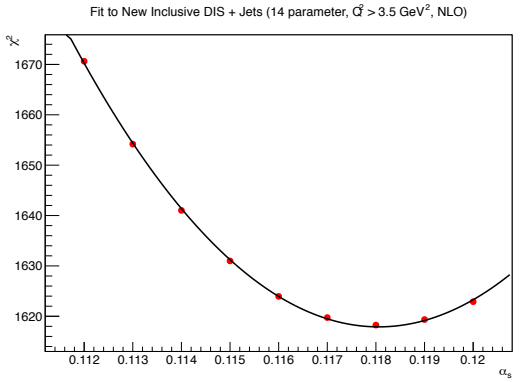

(b) α_s-scan using 14 parameter, $Q^2 > 3.5$ GeV^2 and NLO calculation. The jet data increases the sensitivity to α_s such that a quadratic fit to the points with a reasonable result is possible. The fit leads to $\alpha_s = 0.11806 \pm 0.00084$.

Figure 3: Comparison between α_s-scans with and without jet data.

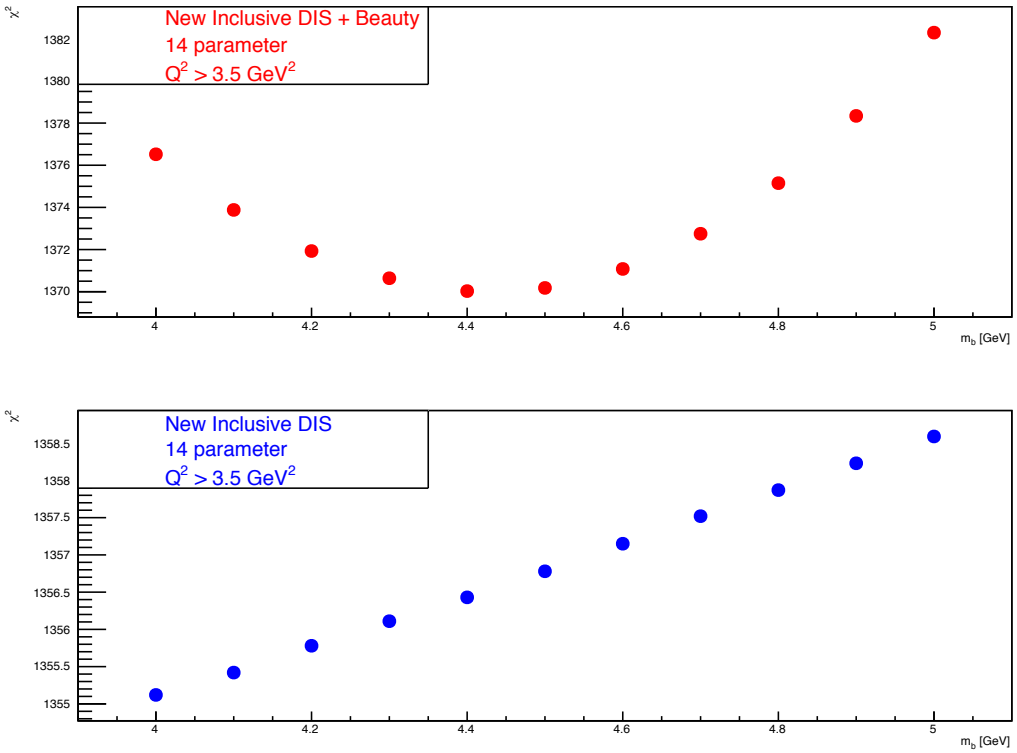

Figure 4: Comparison of m_{b}-scans using inclusive and beauty data and using inclusive data only. One can see very nicely that the scan without the beauty data shows very low sensitivity as there is only a straight line. If one would scale the χ^2-axis of the second plot to the range of the first the slope of the line would be even smaller by factor of roughly 4.

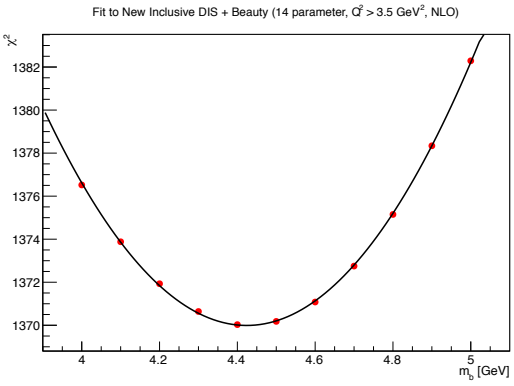

(a) m_{b}-scan using 14 parameter, $Q^2 > 3.5$ GeV^2 and NLO calculation. The result of the fit is $m_{\mathrm{b}} = 4.42 \pm 0.17$.

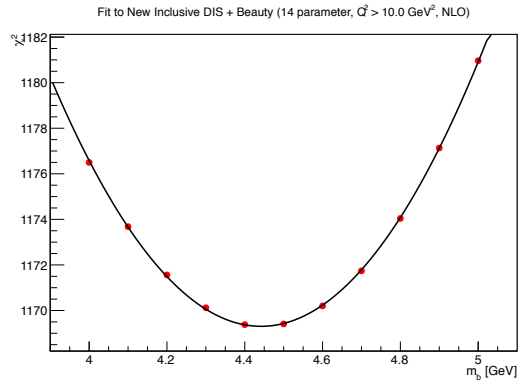

(b) m_{b}-scan using 14 parameter, $Q^2 > 10.0$ GeV^2 and NLO calculation. The result of the fit is $m_{\mathrm{b}} = 4.44 \pm 0.17$.

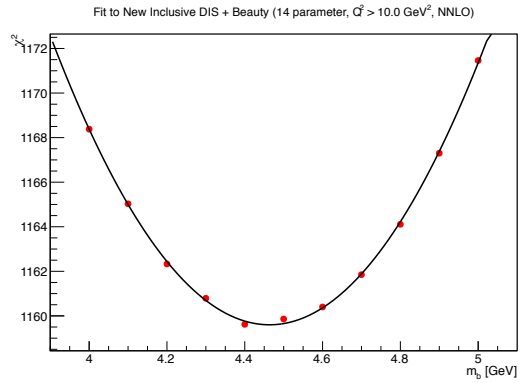

(c) m_{b}-scan using 14 parameter, $Q^2 > 10.0$ GeV^2 and NNLO calculation. The result of the fit is $m_{\mathrm{b}} = 4.46 \pm 0.16$.

Figure 5: m_{b}-scans made with 14 parameter.

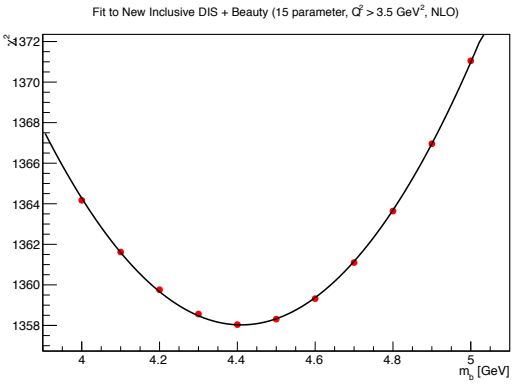

(a) m_{b}-scan using 15 parameter, $Q^2 > 3.5$ GeV^2 and NLO calculation. The result of the fit is $m_{\mathrm{b}} = 4.41 \pm 0.17$.

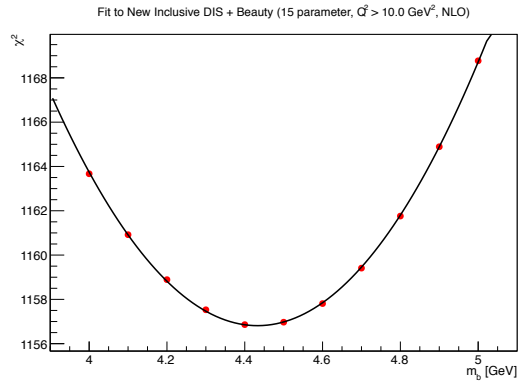

(b) m_{b}-scan using 15 parameter, $Q^2 > 10.0$ GeV^2 and NLO calculation. The result of the fit is $m_{\mathrm{b}} = 4.43 \pm 0.17$.

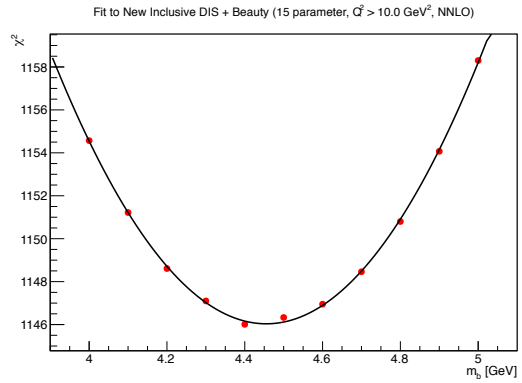

(c) m_{b}-scan using 15 parameter, $Q^2 > 10.0$ GeV^2 and NNLO calculation. The result of the fit is $m_{\mathrm{b}} = 4.46 \pm 0.16$.

Figure 6: m_{b}-scans made with 15 parameter.

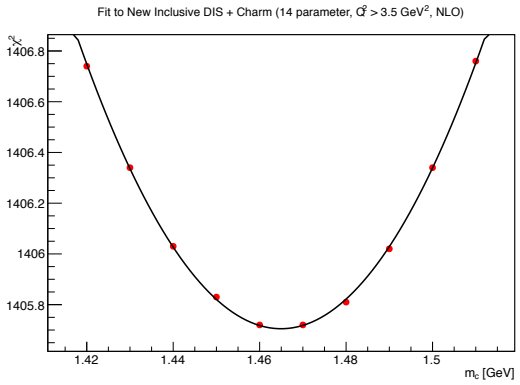

(a) m_c-scan using 14 parameter, $Q^2 > 3.5$ GeV^2 and NLO calculation. The result of the fit is $m_c = 1.465 \pm 0.045$.

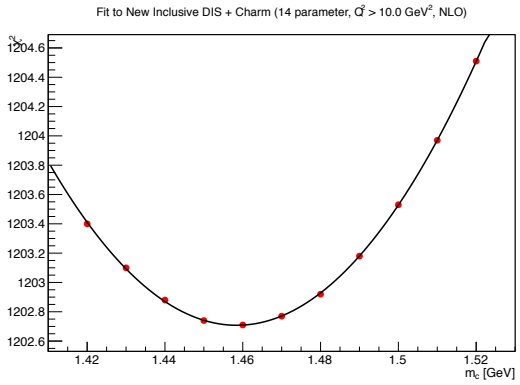

(b) m_c-scan using 14 parameter, $Q^2 > 10.0$ GeV^2 and NLO calculation. The result of the fit is $m_c = 1.458 \pm 0.046$.

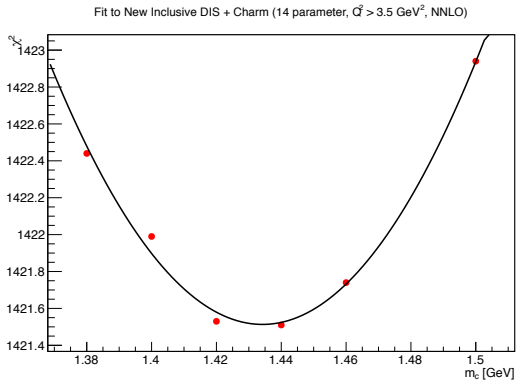

(c) m_c-scan using 14 parameter, $Q^2 > 3.5$ GeV^2 and NNLO calculation. The result of the fit is $m_c = 1.434 \pm 0.056$.

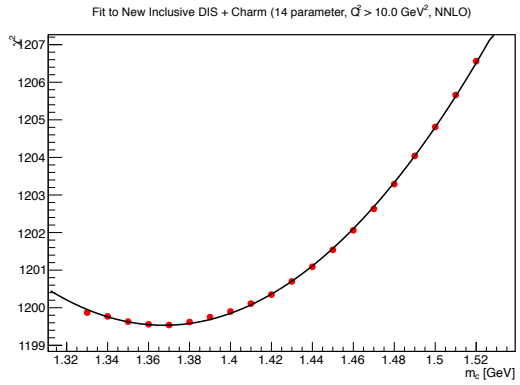

(d) m_c-scan using 14 parameter, $Q^2 > 10.0$ GeV^2 and NNLO calculation. The result of the fit is $m_c = 1.367 \pm 0.058$.

Figure 7: m_c-scans made with 14 parameter.

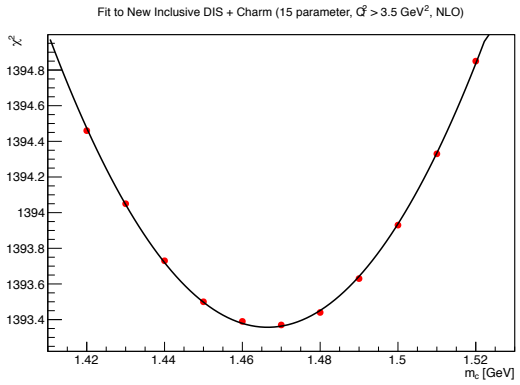

(a) m_c-scan using 15 parameter, $Q^2 > 3.5$ GeV^2 and NLO calculation. The result of the fit is $m_c = 1.466 \pm 0.044$.

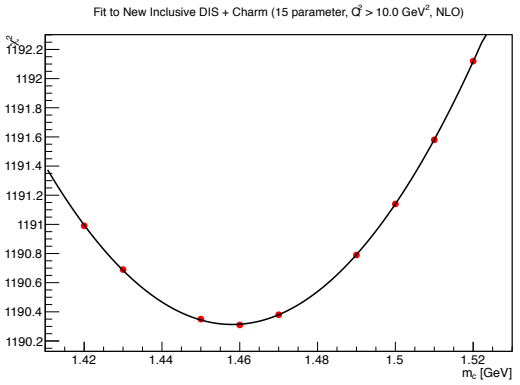

(b) m_c-scan using 15 parameter, $Q^2 > 10.0$ GeV^2 and NLO calculation. The result of the fit is $m_c = 1.458 \pm 0.047$.

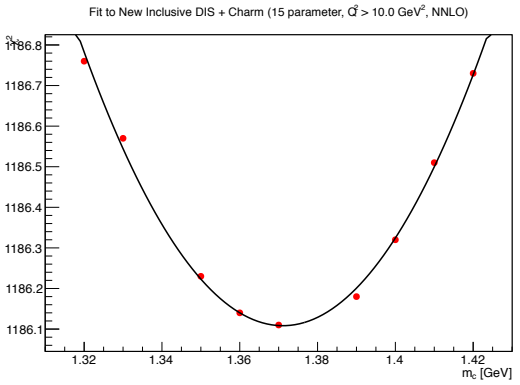

(c) m_c-scan using 15 parameter, $Q^2 > 10.0$ GeV^2 and NNLO calculation. The result of the fit is $m_c = 1.371 \pm 0.063$.

Figure 8: m_c-scans made with 15 parameter.

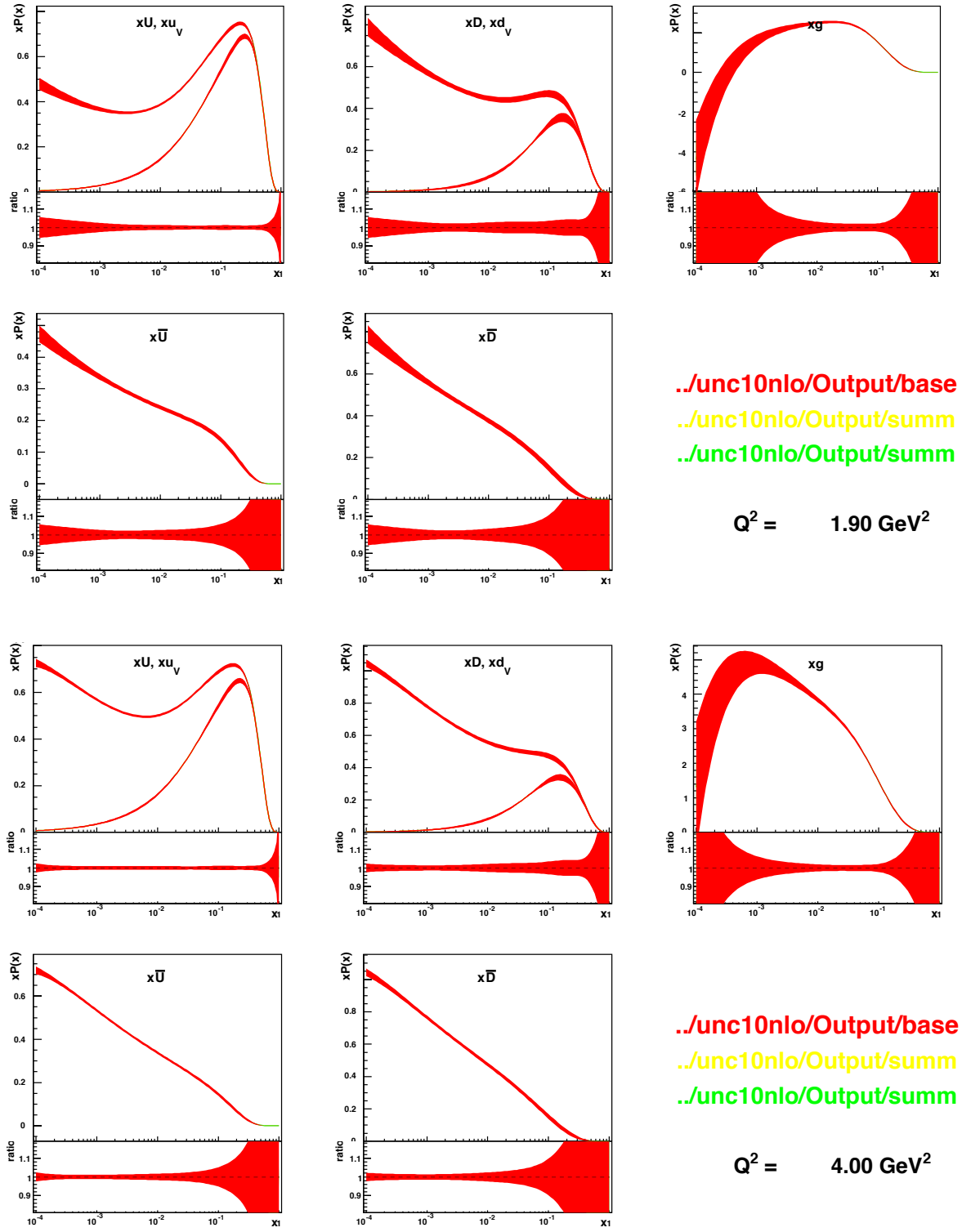

Figure 9: PDF's with experimental (red), model (yellow) and parametrisation (green) uncertainty at different values of Q^2. The fits are done with inclusive data only with a Q^2-cut at 10 GeV^2 and to NLO

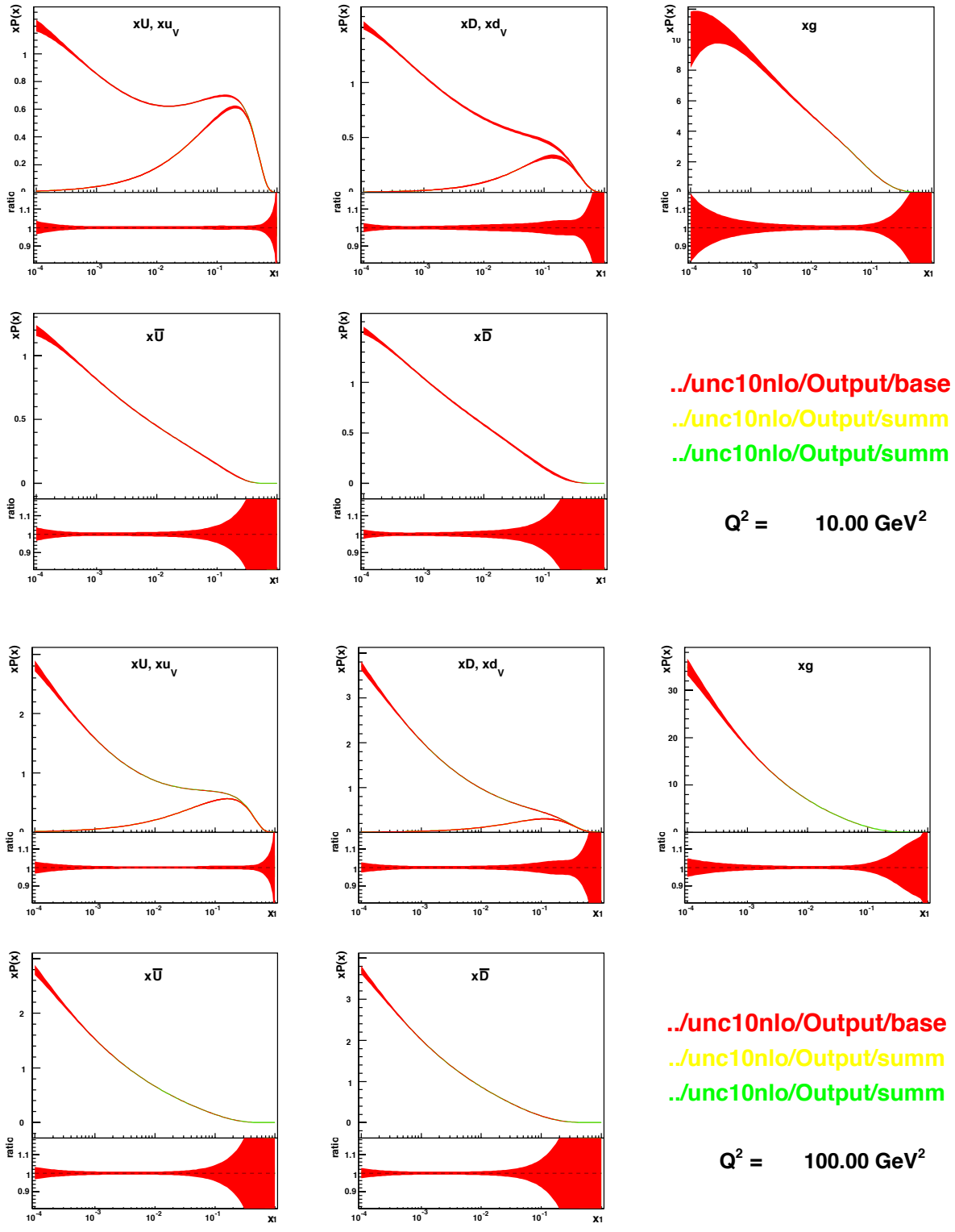

Figure 9: PDF's with experimental (red), model (yellow) and parametrisation (green) uncertainty at different values of Q^2. The fits are done with inclusive data only with a Q^2-cut at 10 GeV^2 and to NLO

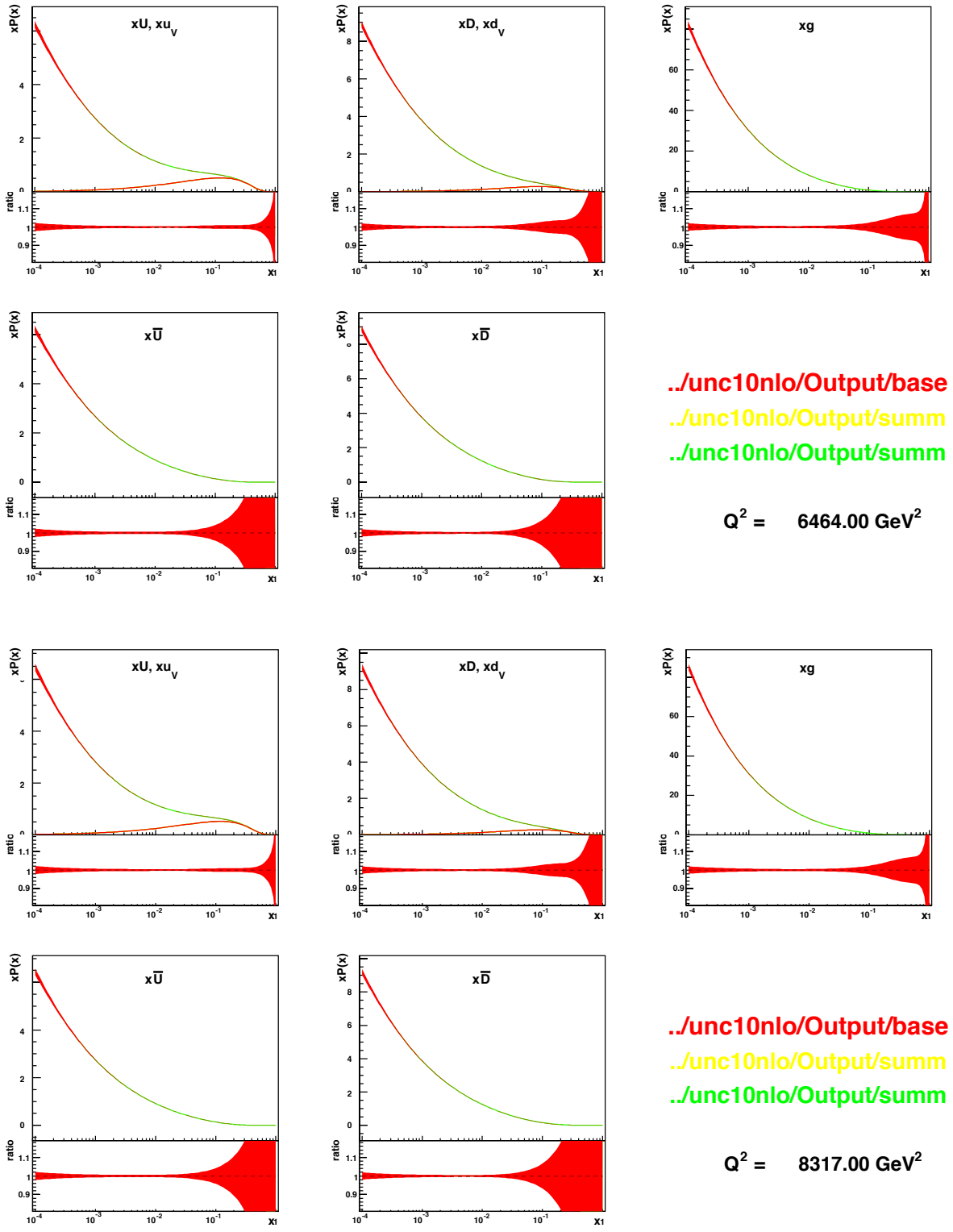

Figure 9: PDF's with experimental (red), model (yellow) and parametrisation (green) uncertainty at different values of Q^2. The fits are done with inclusive data only with a Q^2-cut at 10 GeV^2 and to NLO

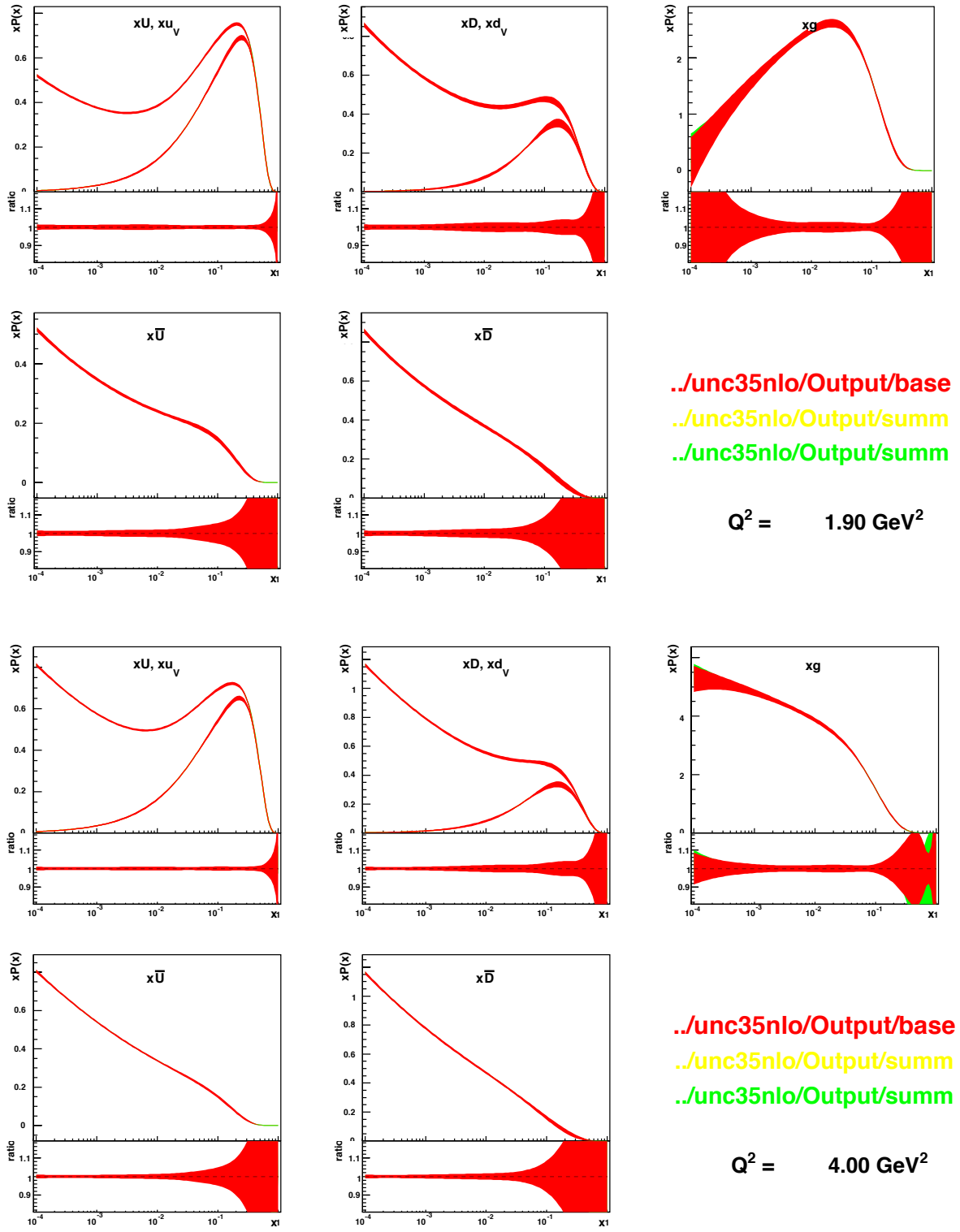

Figure 10: PDF's with experimental (red), model (yellow) and parametrisation (green) uncertainty at different values of Q^2. The fits are done with inclusive data only with a Q^2-cut at 3.5 GeV^2 and to NLO

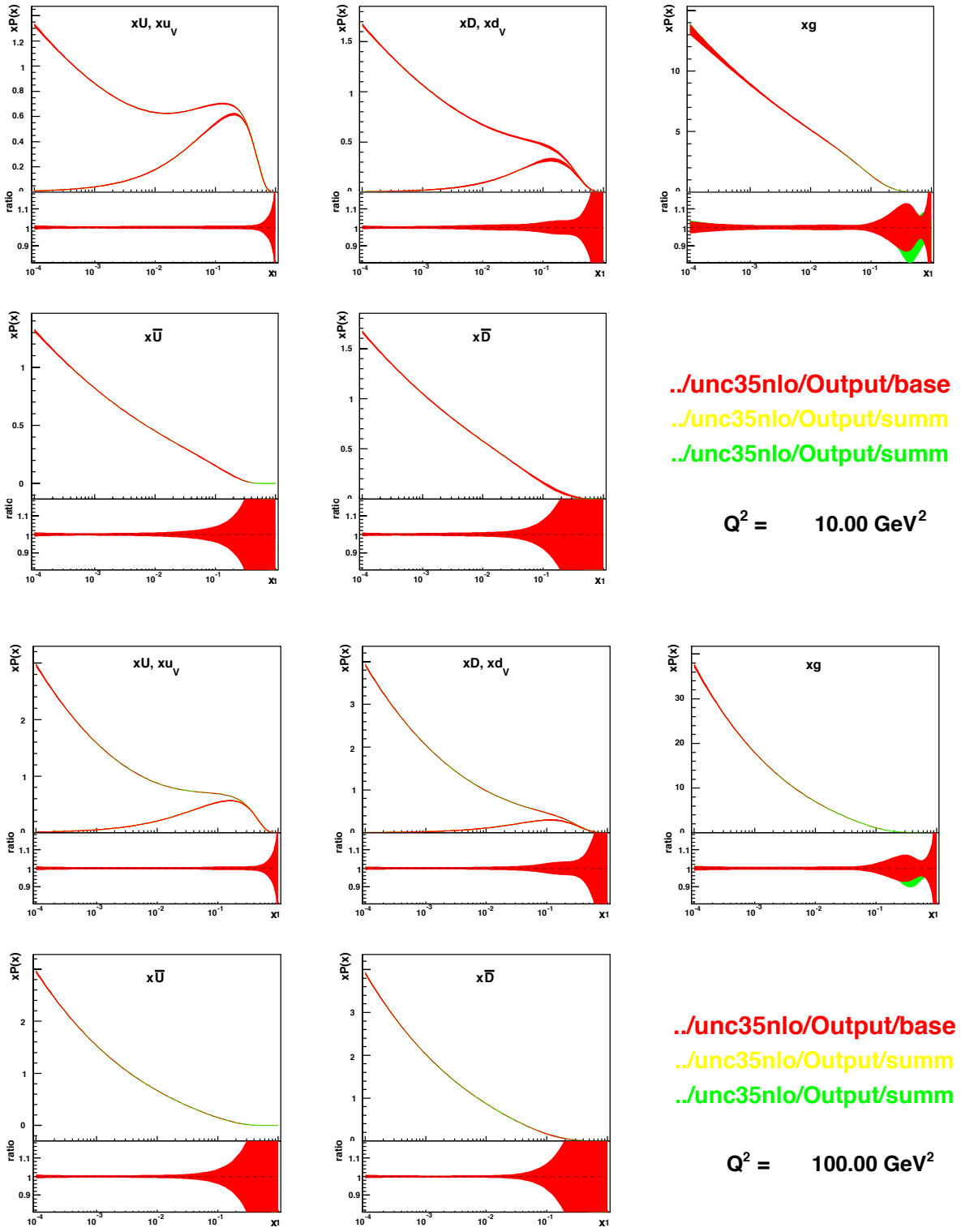

Figure 10: PDF's with experimental (red), model (yellow) and parametrisation (green) uncertainty at different values of Q^2. The fits are done with inclusive data only with a Q^2-cut at 3.5 GeV^2 and to NLO

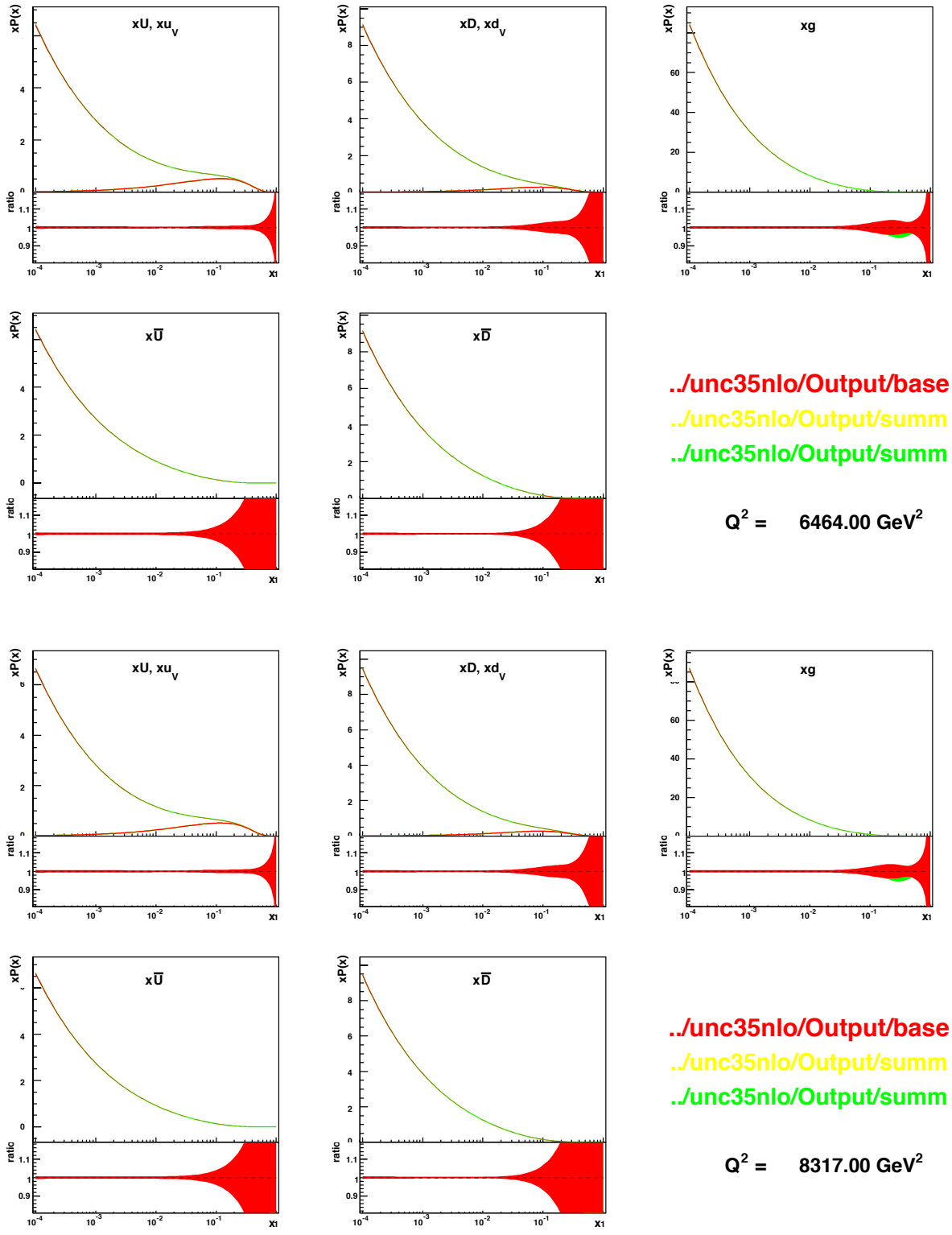

Figure 10: PDF's with experimental (red), model (yellow) and parametrisation (green) uncertainty at different values of Q^2. The fits are done with inclusive data only with a Q^2-cut at 3.5 GeV^2 and to NLO

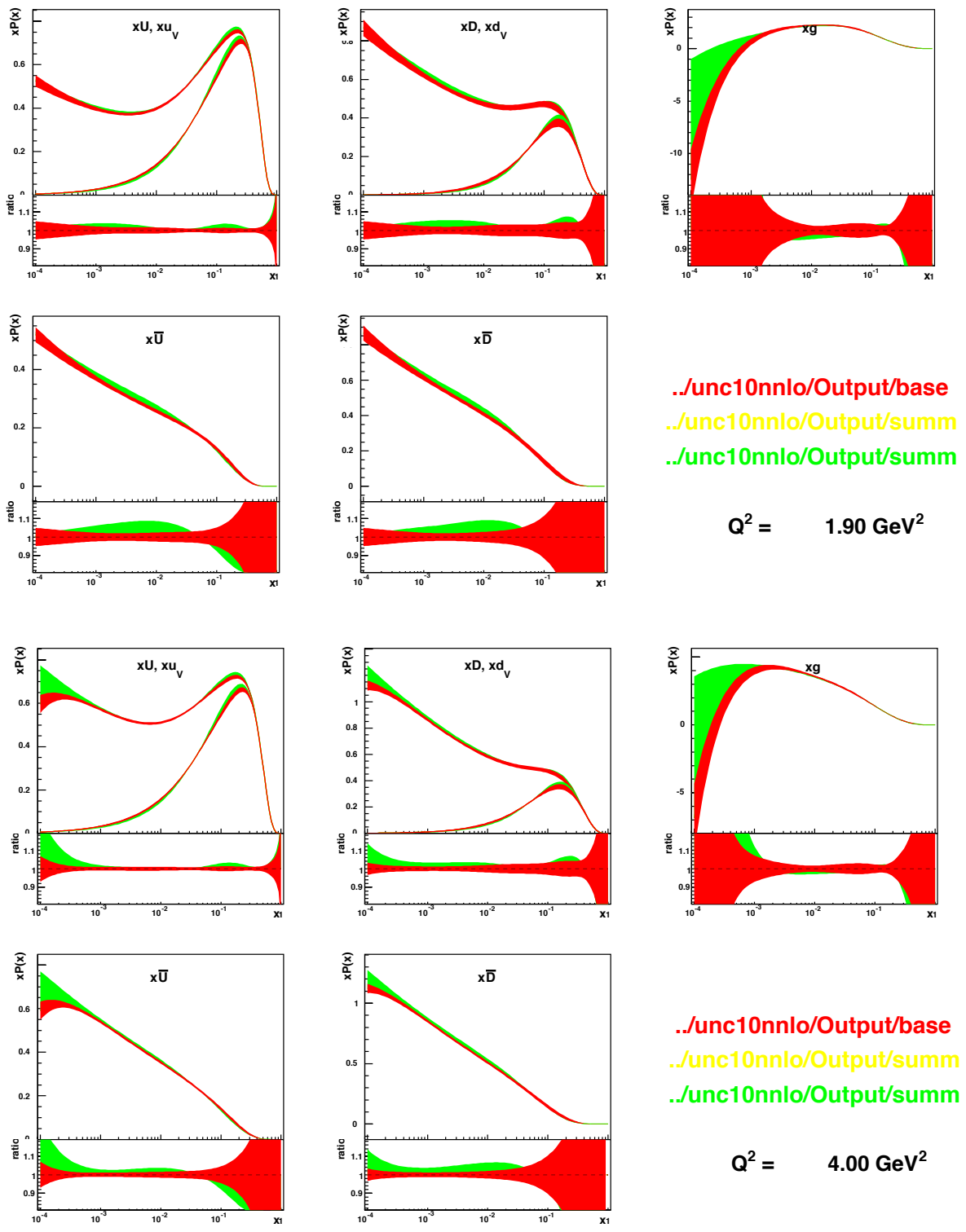

Figure 11: PDF's with experimental (red), model (yellow) and parametrisation (green) uncertainty at different values of Q^2. The fits are done with inclusive data only with a Q^2-cut at 10 GeV^2 and to NNLO

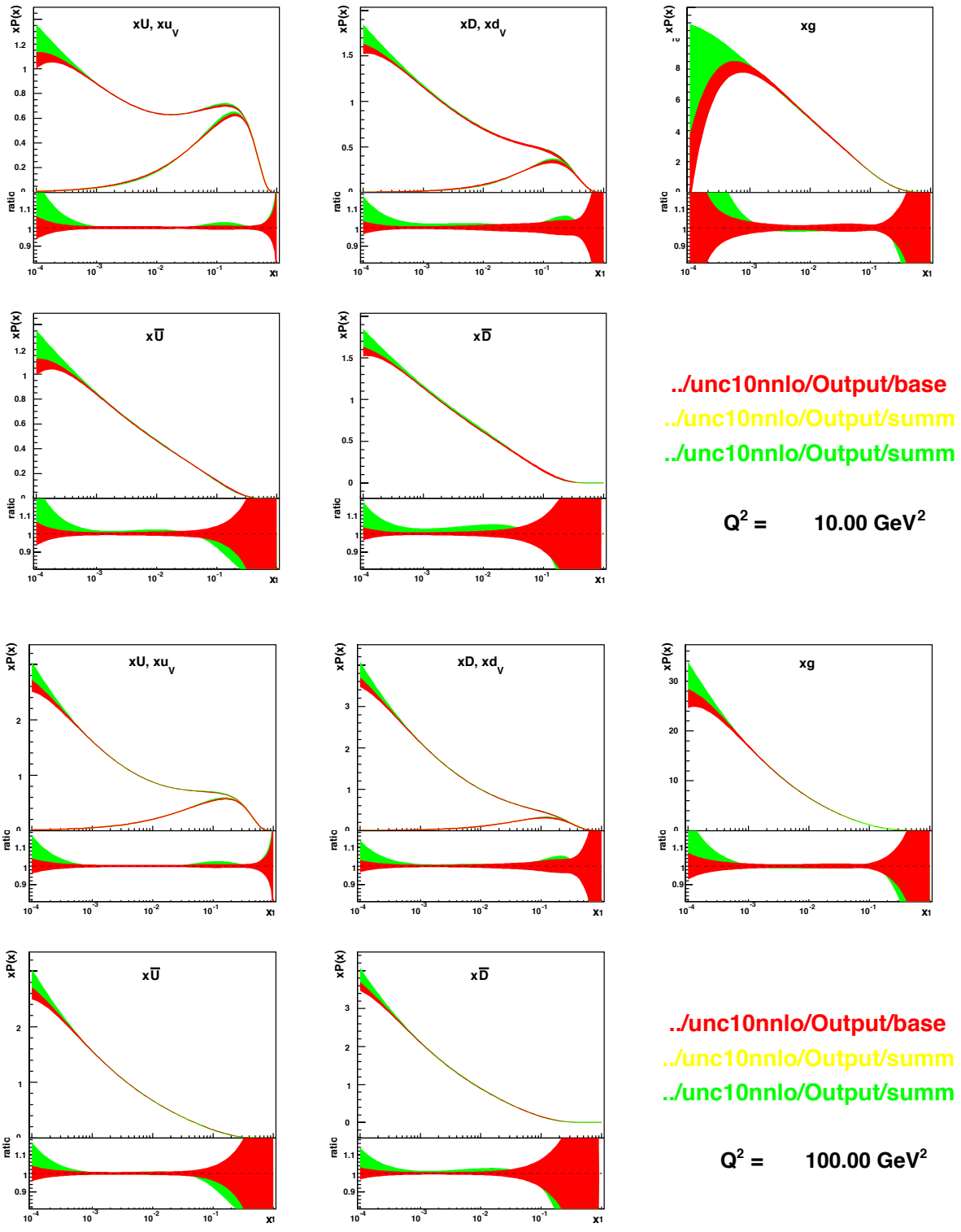

Figure 11: PDF's with experimental (red), model (yellow) and parametrisation (green) uncertainty at different values of Q^2. The fits are done with inclusive data only with a Q^2-cut at 10 GeV^2 and to NNLO

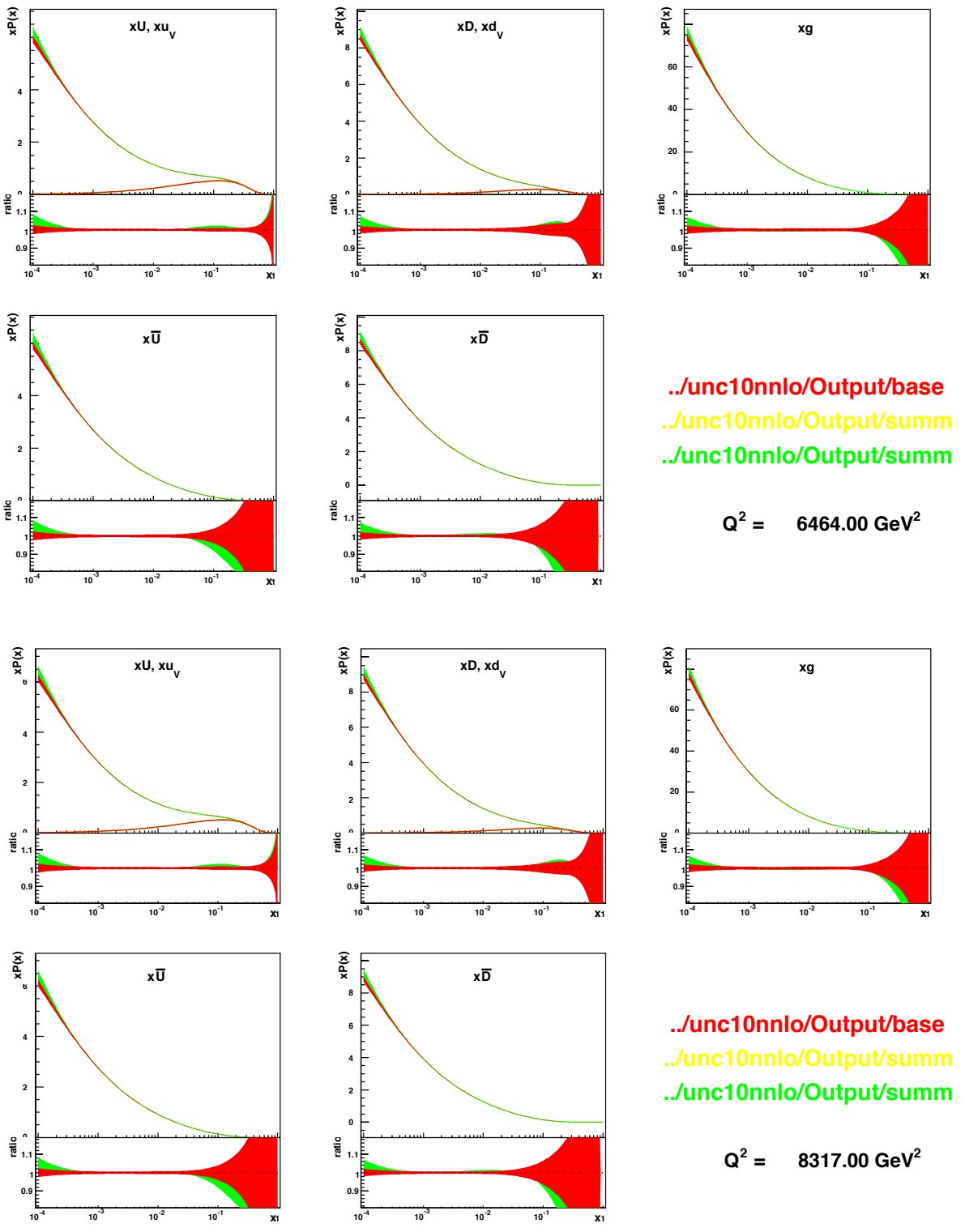

Figure 11: PDF's with experimental (red), model (yellow) and parametrisation (green) uncertainty at different values of Q^2. The fits are done with inclusive data only with a Q^2-cut at 10 GeV^2 and to NNLO

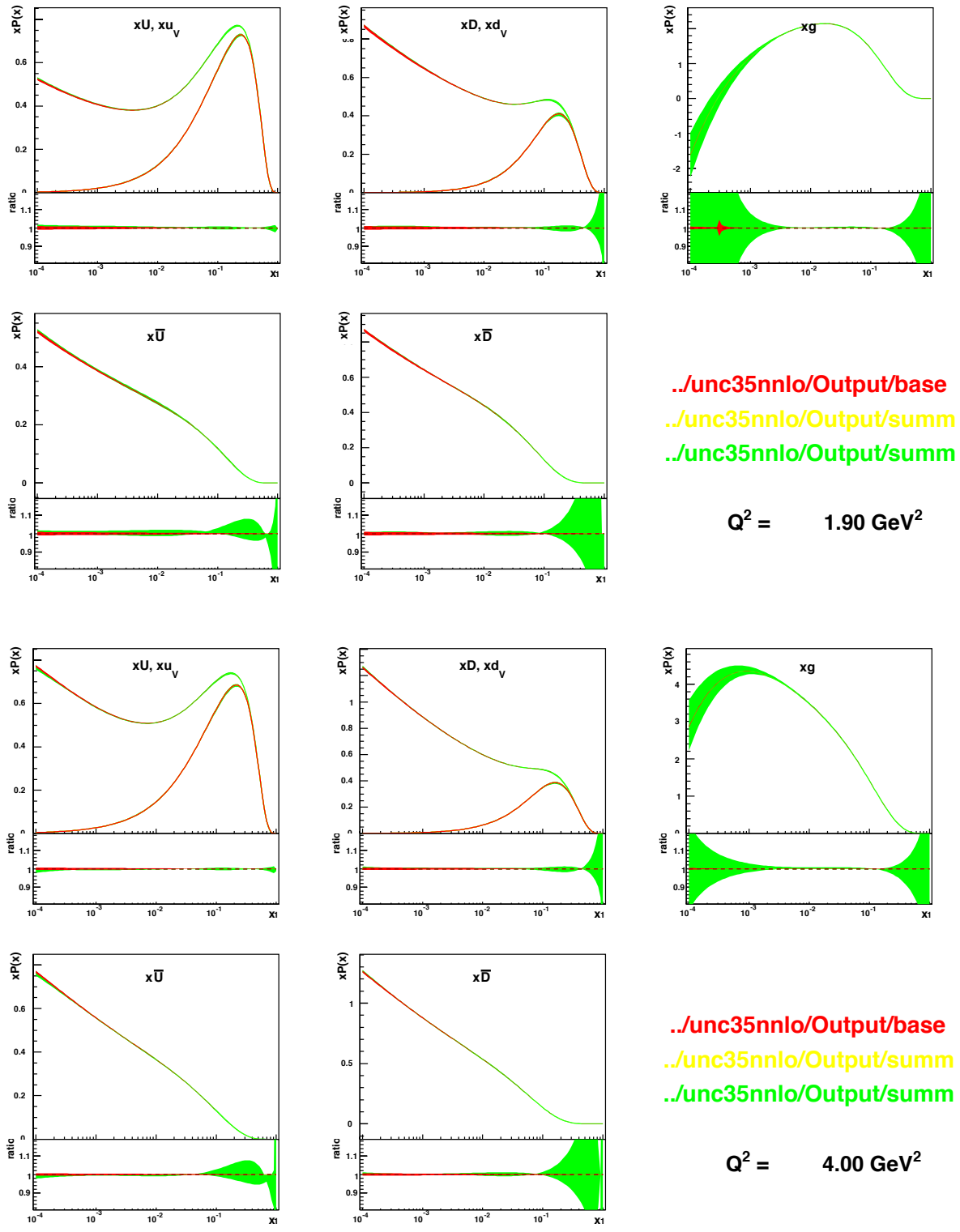

Figure 12: PDF's with experimental (red), model (yellow) and parametrisation (green) uncertainty at different values of Q^2. The fits are done with inclusive data only with a Q^2-cut at 3.5 GeV^2 and to NNLO

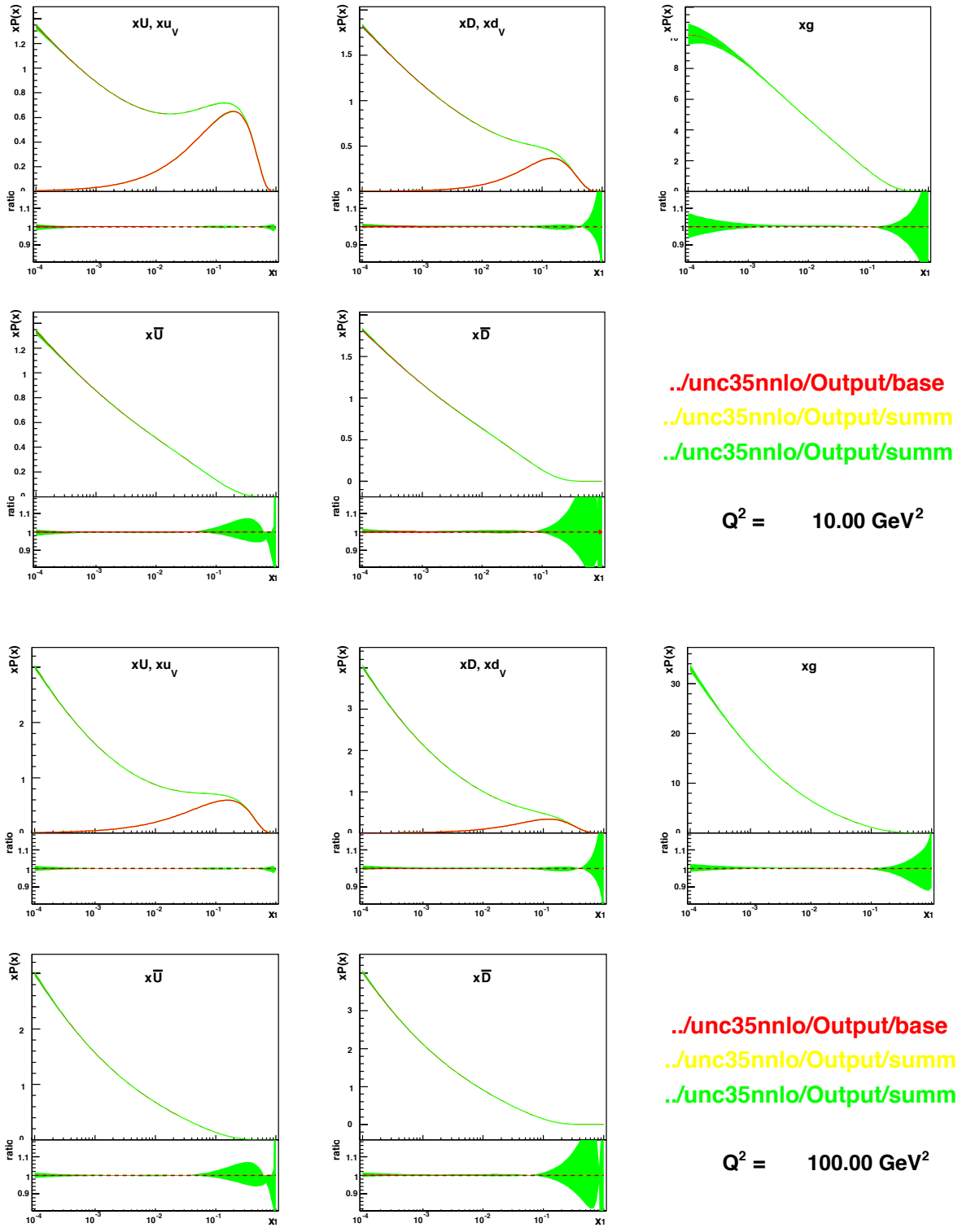

Figure 12: PDF's with experimental (red), model (yellow) and parametrisation (green) uncertainty at different values of Q^2. The fits are done with inclusive data only with a Q^2-cut at 3.5 GeV^2 and to NNLO

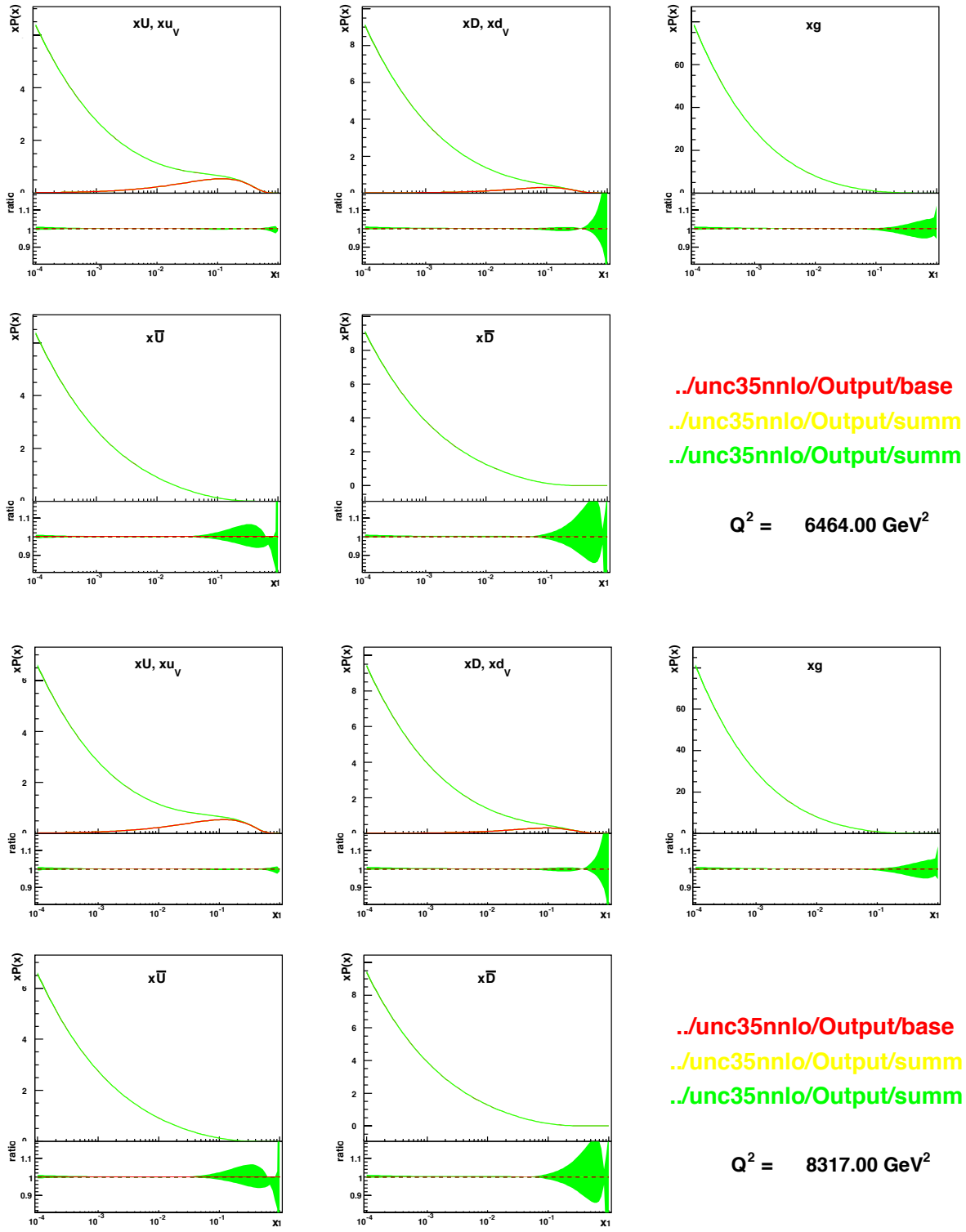

Figure 12: PDF's with experimental (red), model (yellow) and parametrisation (green) uncertainty at different values of Q^2. The fits are done with inclusive data only with a Q^2-cut at 3.5 GeV^2 and to NNLO

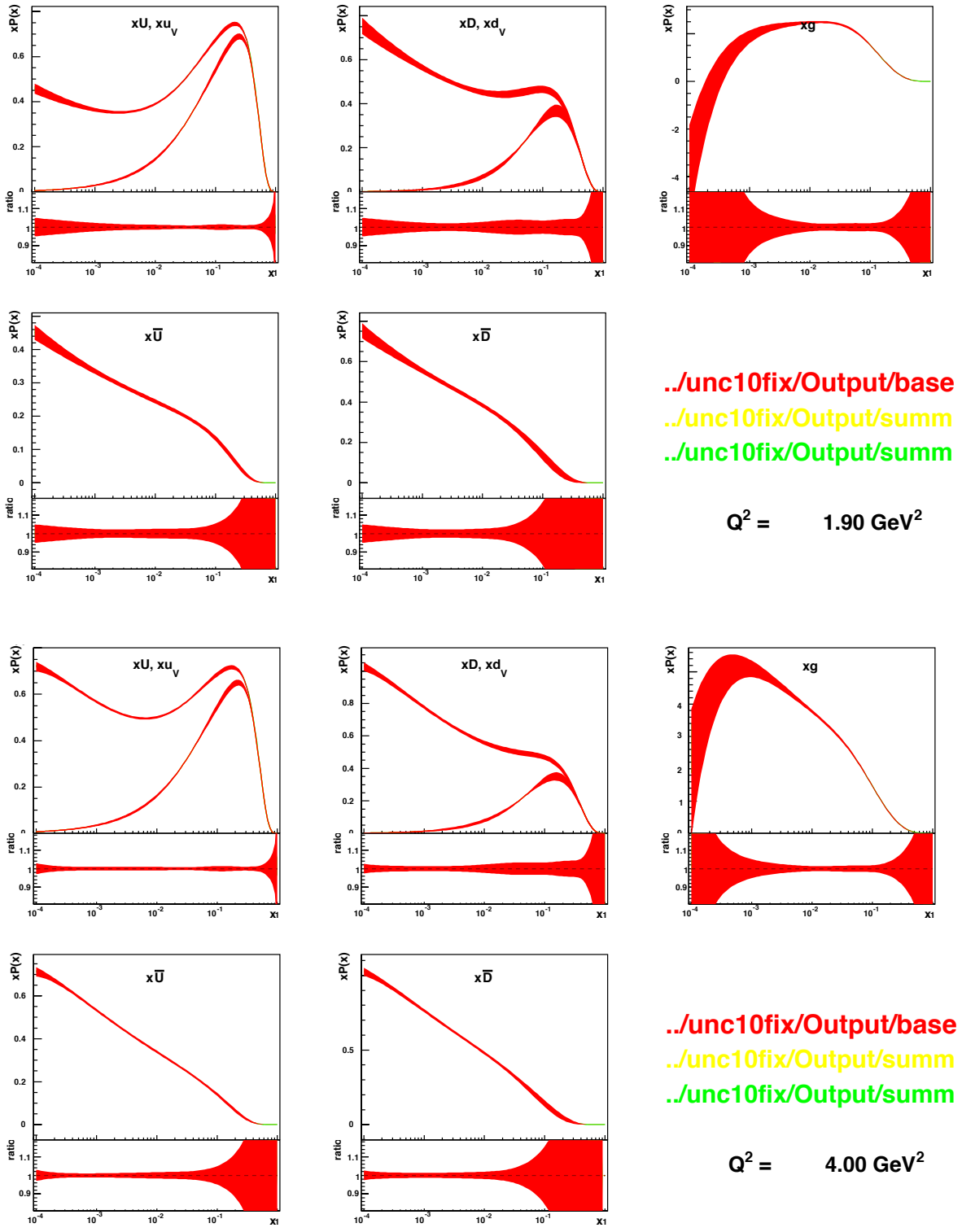

Figure 13: PDF's with experimental (red), model (yellow) and parametrisation (green) uncertainty at different values of Q^2. The fits are done with inclusive, charm and jet data with a Q^2-cut at 10 GeV^2, to NLO and with fixed α_s

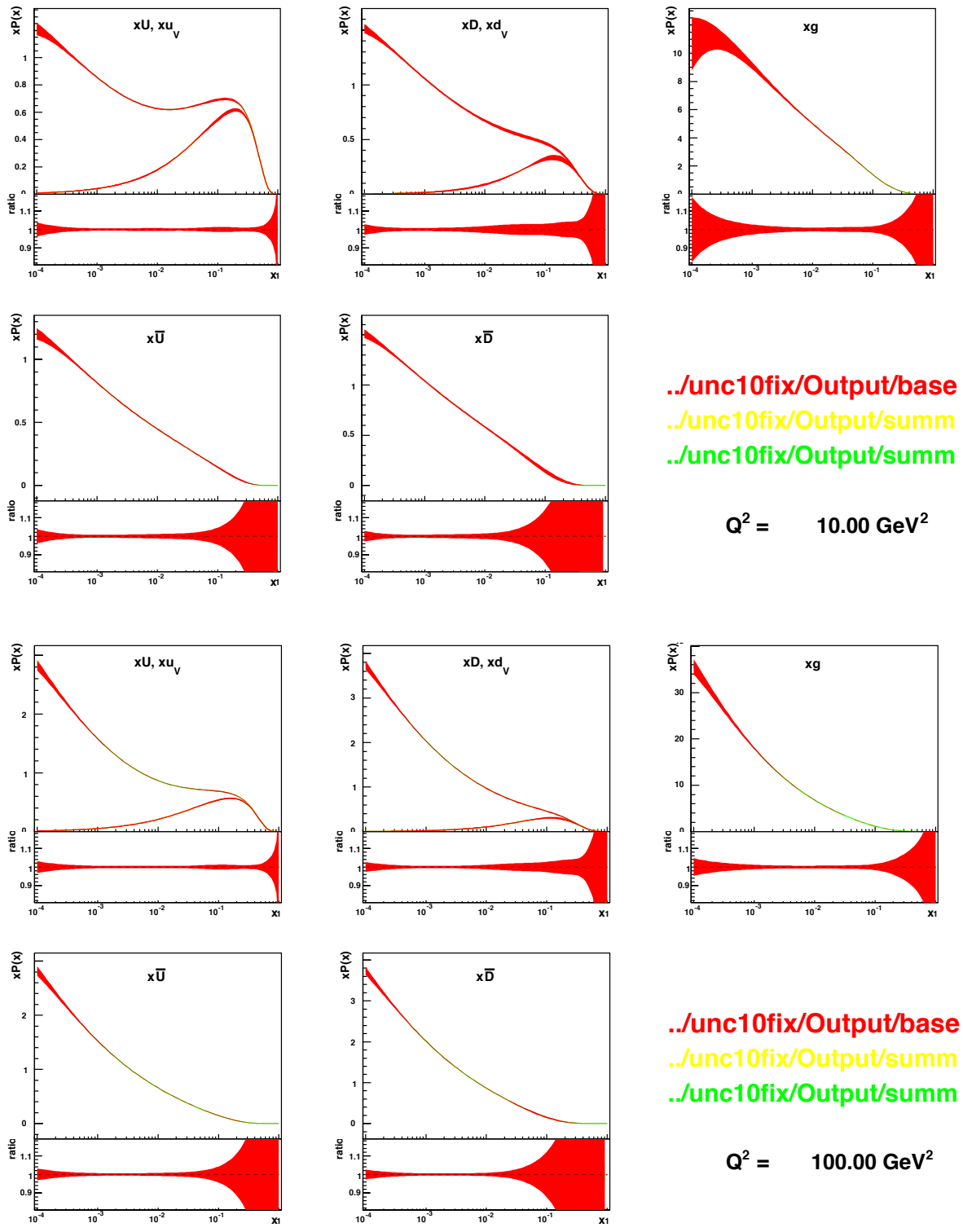

Figure 13: PDF's with experimental (red), model (yellow) and parametrisation (green) uncertainty at different values of Q^2. The fits are done with inclusive, charm and jet data with a Q^2-cut at 10 GeV^2, to NLO and with fixed α_s

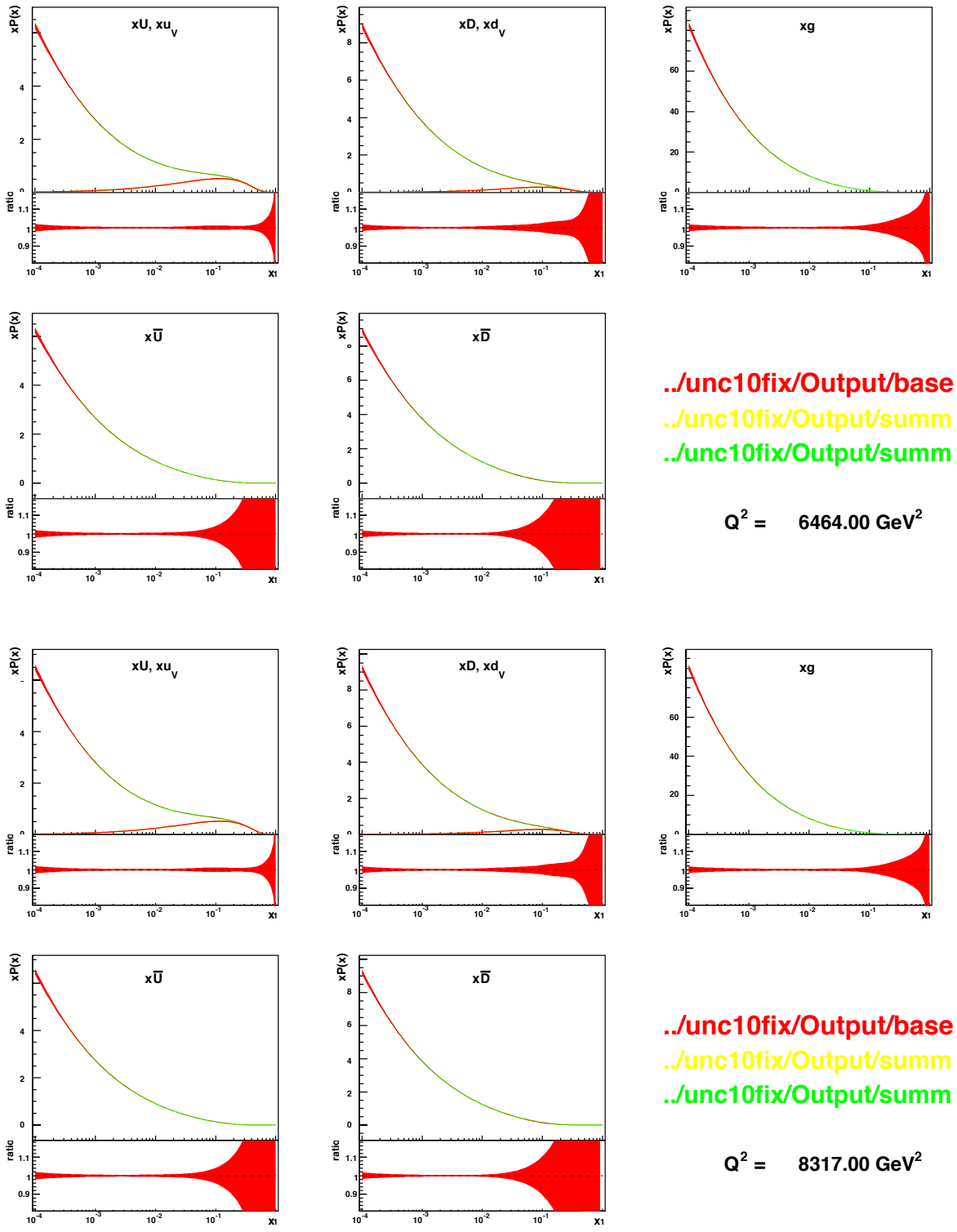

Figure 13: PDF's with experimental (red), model (yellow) and parametrisation (green) uncertainty at different values of Q^2. The fits are done with inclusive, charm and jet data with a Q^2-cut at 10 GeV^2, to NLO and with fixed α_s

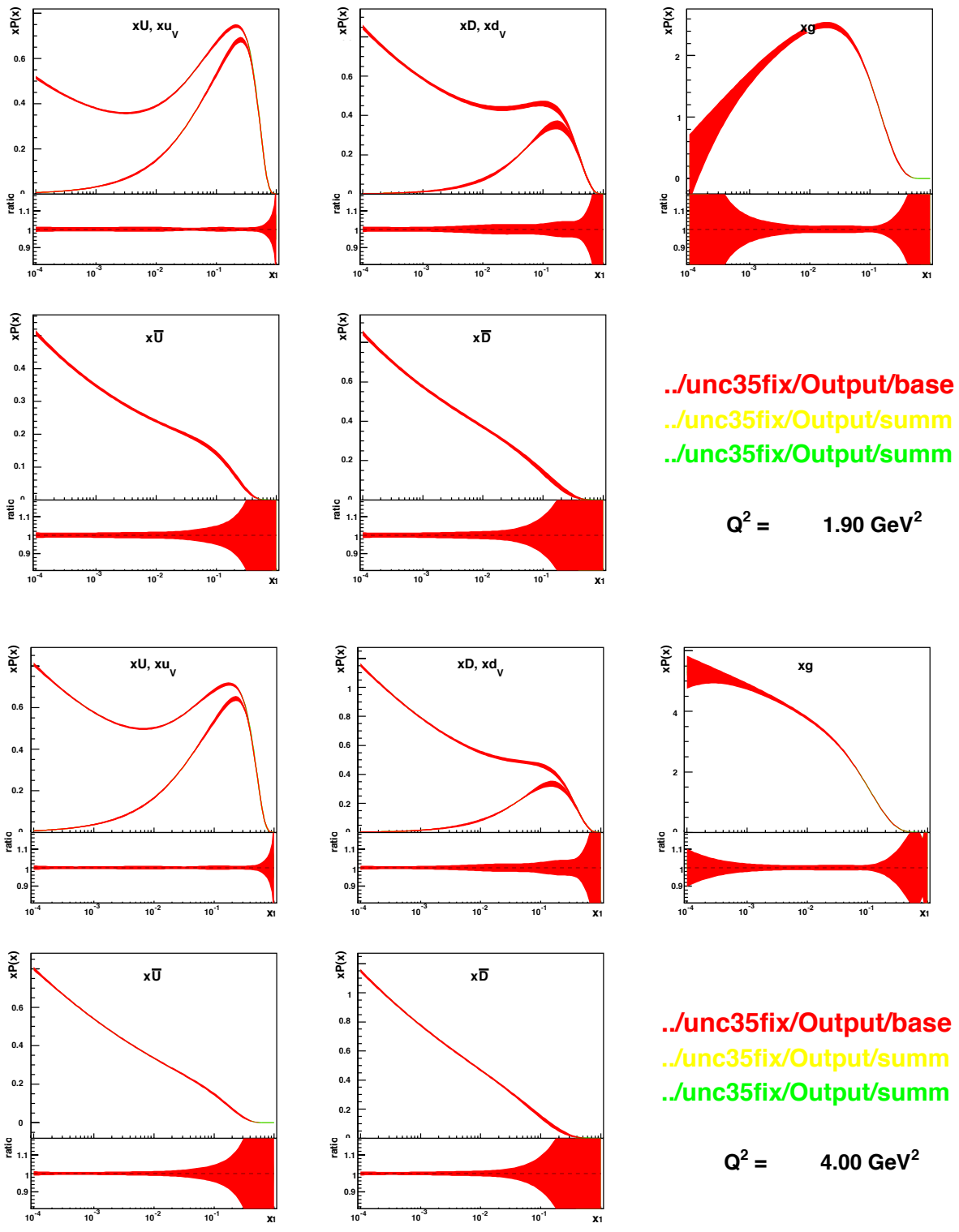

Figure 14: PDF's with experimental (red), model (yellow) and parametrisation (green) uncertainty at different values of Q^2. The fits are done with inclusive, charm and jet data with a Q^2-cut at 3.5 GeV^2, to NLO and with fixed α_s

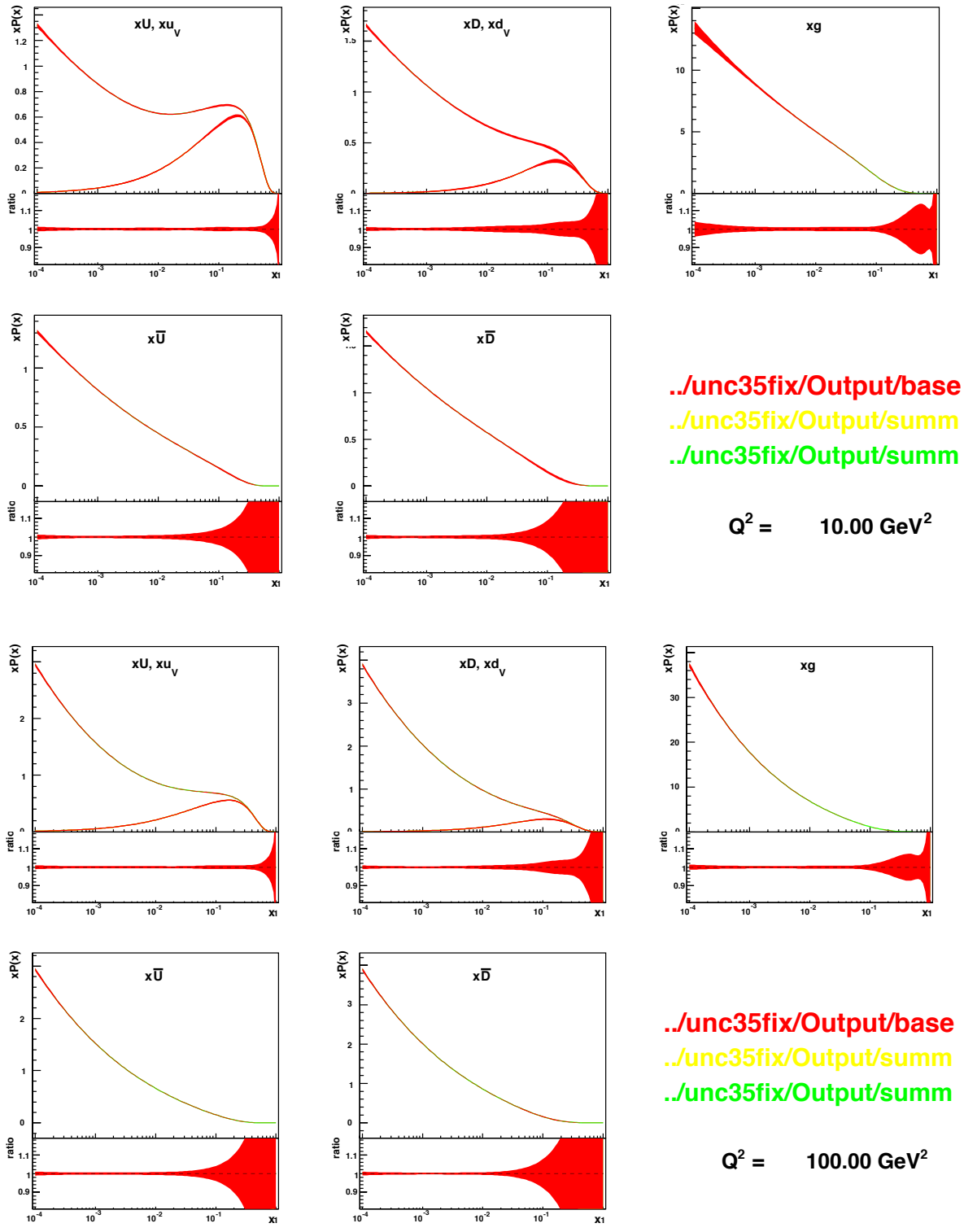

Figure 14: PDF's with experimental (red), model (yellow) and parametrisation (green) uncertainty at different values of Q^2. The fits are done with inclusive, charm and jet data with a Q^2-cut at 3.5 GeV^2, to NLO and with fixed α_s

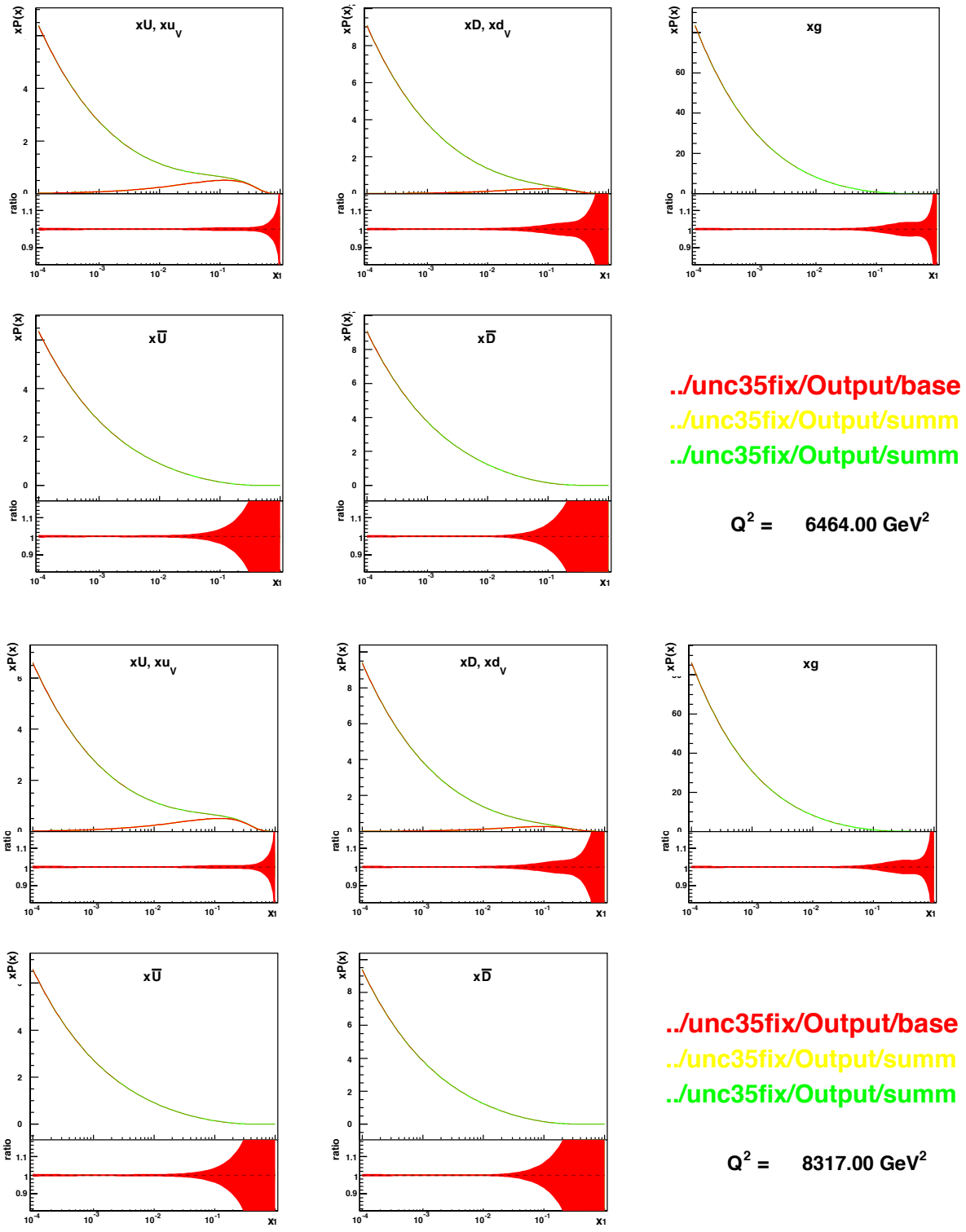

Figure 14: PDF's with experimental (red), model (yellow) and parametrisation (green) uncertainty at different values of Q^2. The fits are done with inclusive, charm and jet data with a Q^2-cut at 3.5 GeV^2, to NLO and with fixed α_s

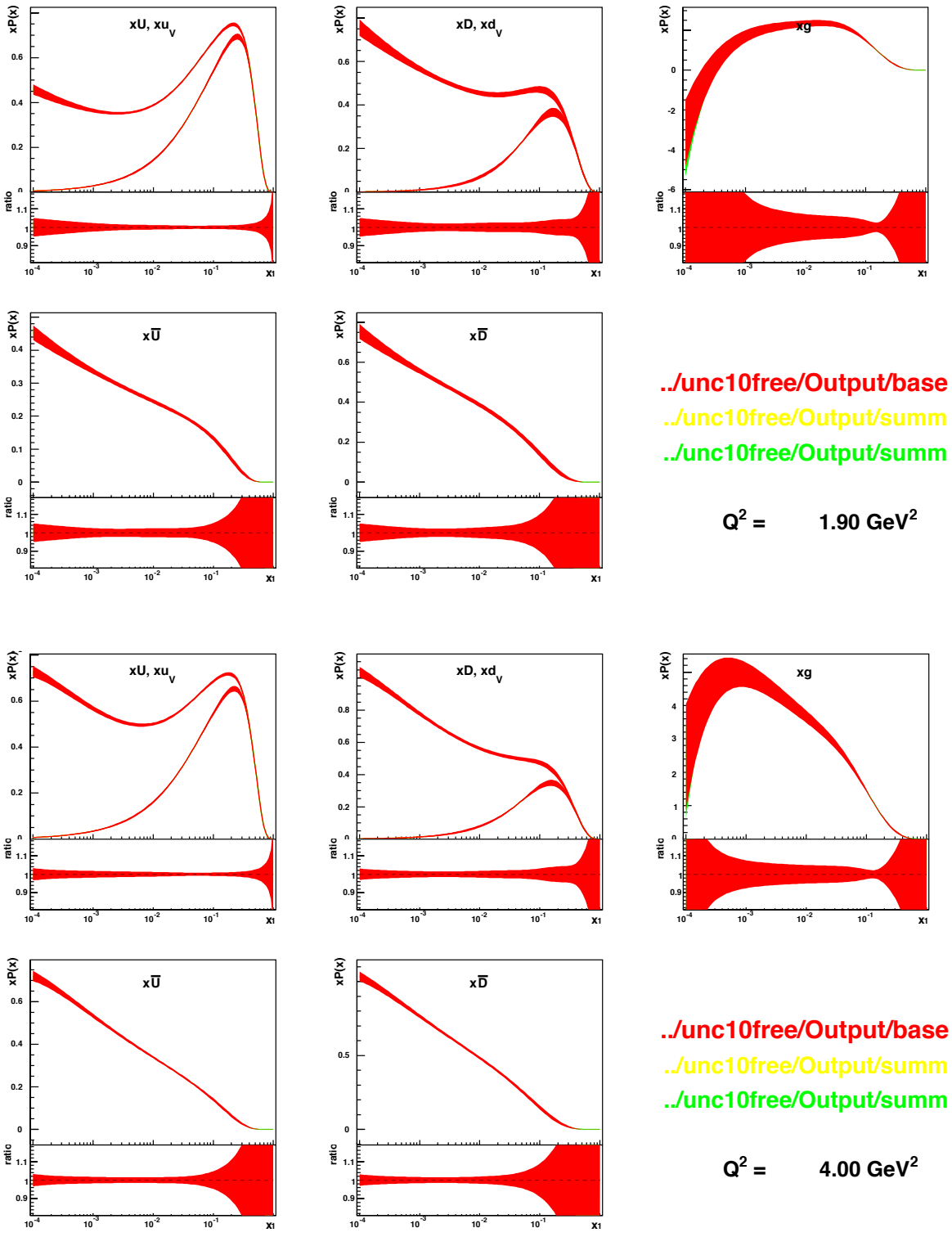

Figure 15: PDF's with experimental (red), model (yellow) and parametrisation (green) uncertainty at different values of Q^2. The fits are done with inclusive, charm and jet data with a Q^2-cut at 10 GeV^2, to NLO and with free α_s

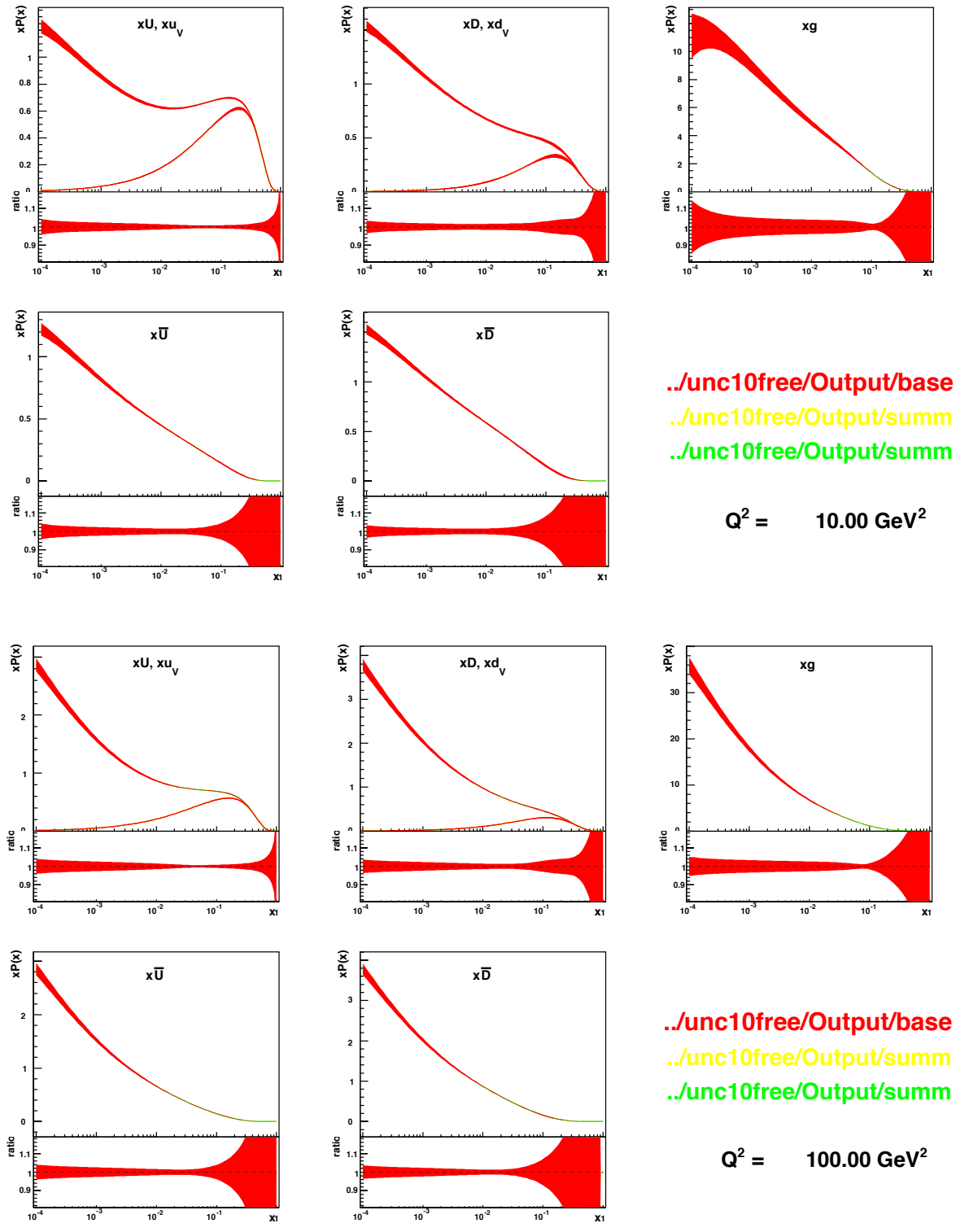

Figure 15: PDF's with experimental (red), model (yellow) and parametrisation (green) uncertainty at different values of Q^2. The fits are done with inclusive, charm and jet data with a Q^2-cut at 10 GeV^2, to NLO and with free α_s

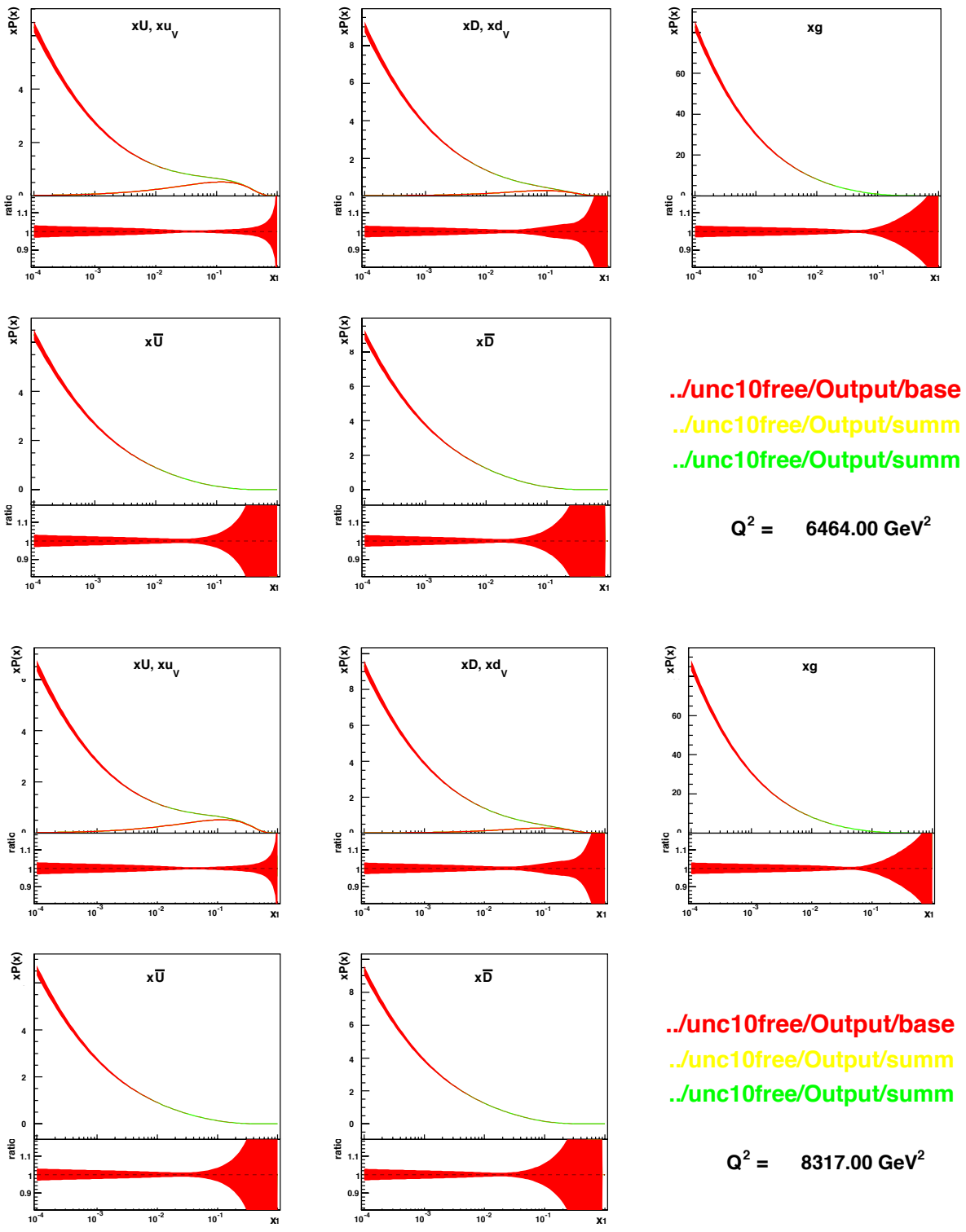

Figure 15: PDF's with experimental (red), model (yellow) and parametrisation (green) uncertainty at different values of Q^2. The fits are done with inclusive, charm and jet data with a Q^2-cut at 10 GeV^2, to NLO and with free α_s

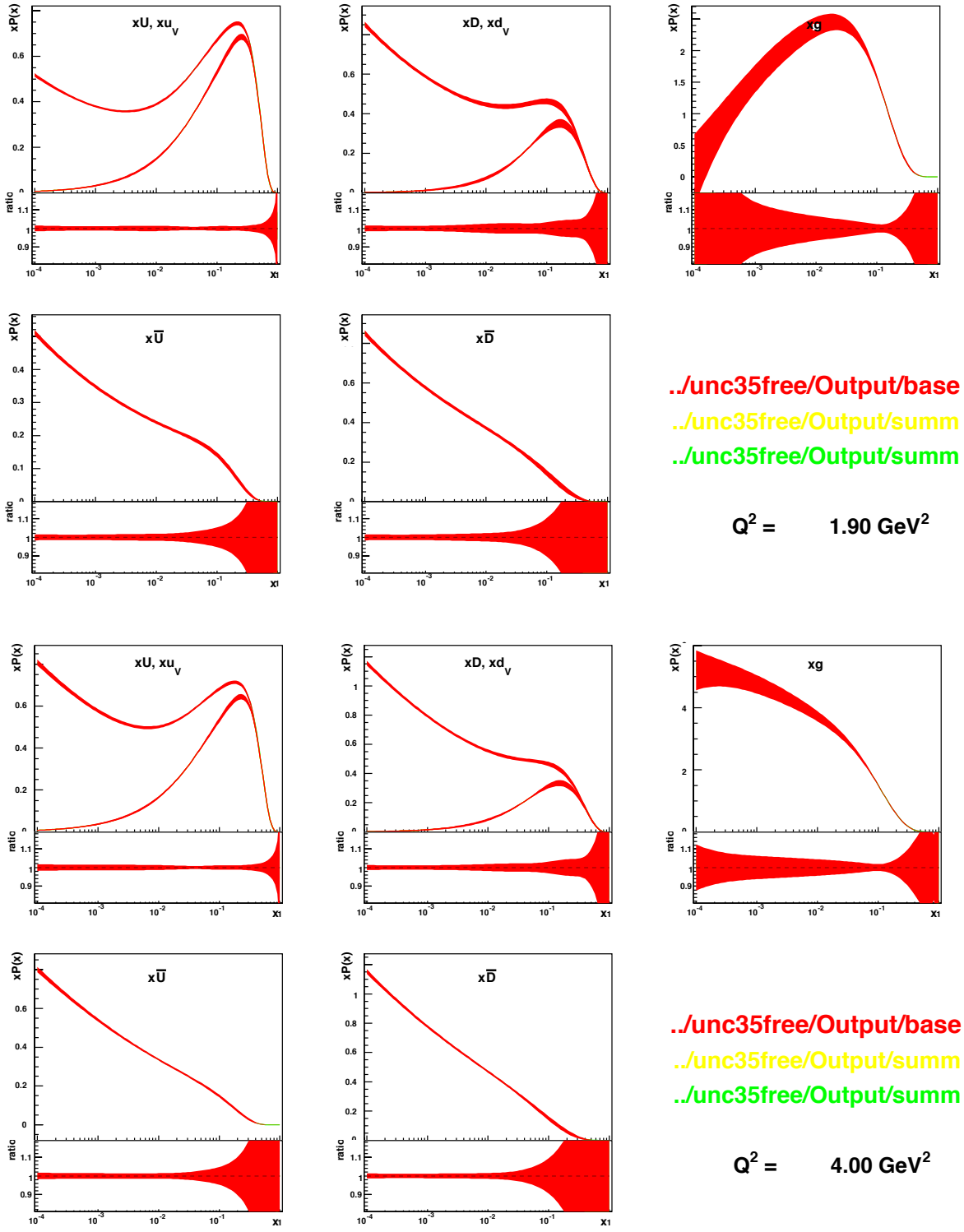

Figure 16: PDF's with experimental (red), model (yellow) and parametrisation (green) uncertainty at different values of Q^2. The fits are done with inclusive, charm and jet data with a Q^2-cut at 3.5 GeV^2, to NLO and with free α_s

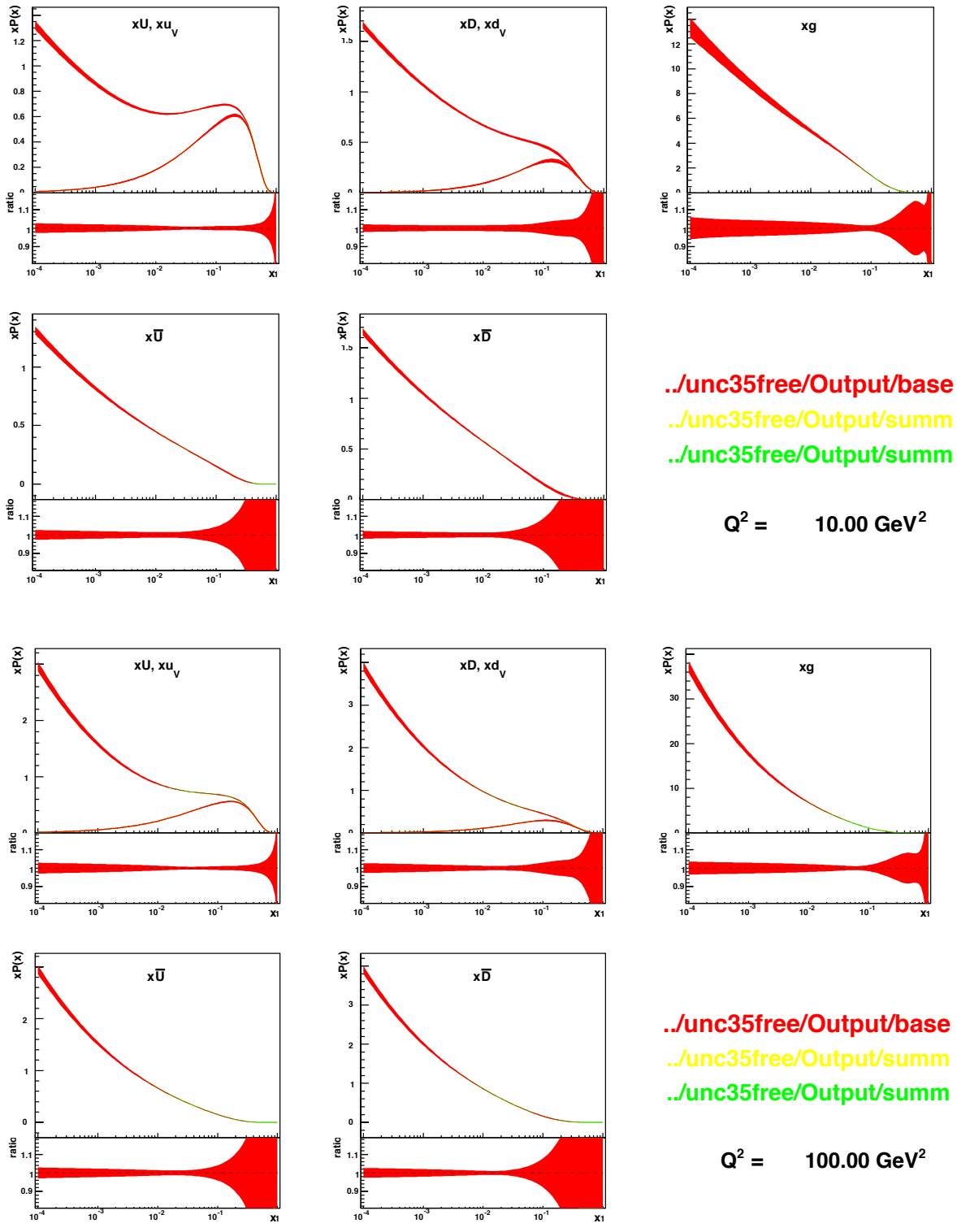

Figure 16: PDF's with experimental (red), model (yellow) and parametrisation (green) uncertainty at different values of Q^2. The fits are done with inclusive, charm and jet data with a Q^2-cut at 3.5 GeV^2, to NLO and with free α_s

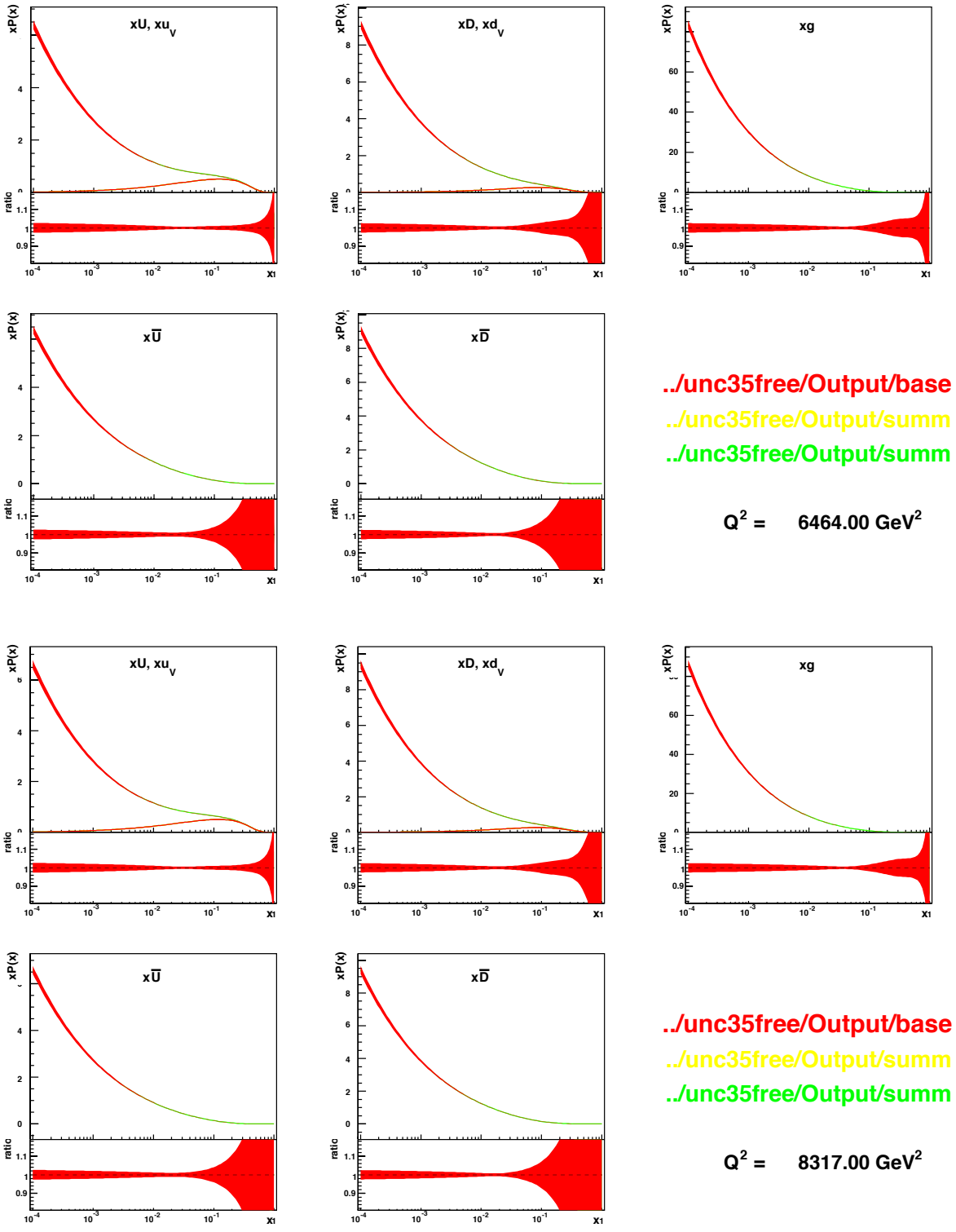

Figure 16: PDF's with experimental (red), model (yellow) and parametrisation (green) uncertainty at different values of Q^2. The fits are done with inclusive, charm and jet data with a Q^2-cut at 3.5 GeV^2, to NLO and with free α_s